110 P

THERMAL SCALE MODELING OF SPACECRAFT: AN EXPERIMENTAL INVESTIGATION

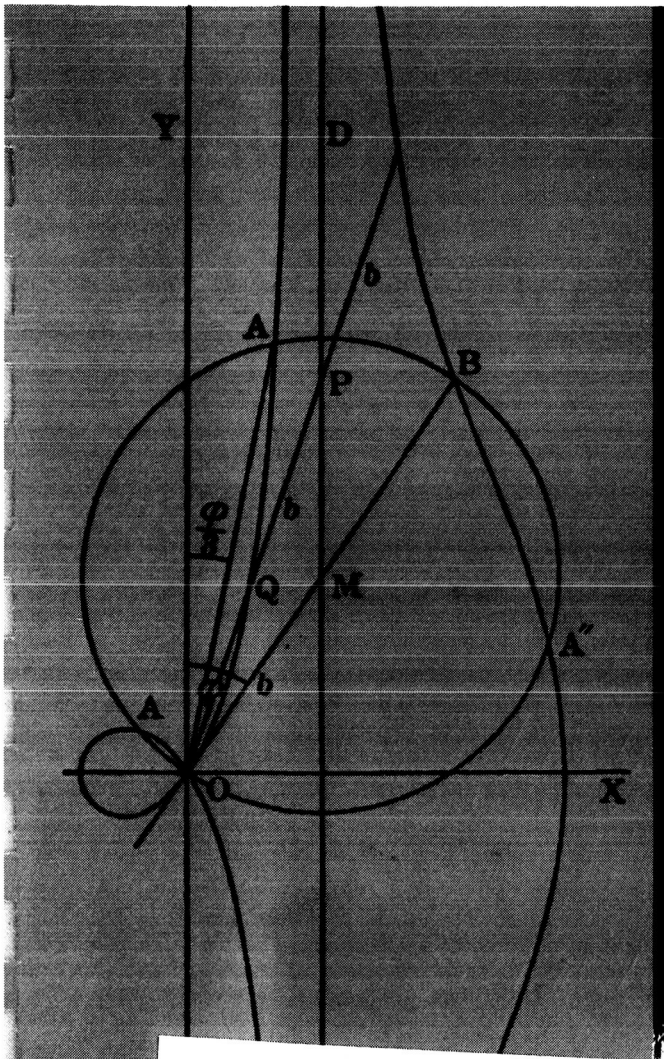

DIVISION OF Arthur D. Little, Inc.

500

PREPARED FOR

JET PROPULSION LABORATORY

CONTRACT NO. 950252

THERMAL SCALE MODELING OF SPACECRAFT: AN EXPERIMENTAL INVESTIGATION

Prepared for

Jet Propulsion Laboratory
4800 Oak Grove Drive
Pasadena, California

Contract No. 950252

by

Arthur A. Fowle

Frank Gabron

Robert W. Johnson

C-64924

June 28, 1963

TABLE OF CONTENTS

	Page
List of Tables	iv
List of Figures	v
ACKNOWLEDGEMENTS	vi
SUMMARY	vii
CONCLUSIONS AND RECOMMENDATIONS	ix
INTRODUCTION	xv
I. THE THERMAL MODELING PROBLEM	1
A. INTRODUCTION	1
B. HEAT TRANSPORT BY SOLID CONDUCTION	2
C. HEAT TRANSPORT AT SOLID-TO-SOLID INTERFACES	2
D. HEAT GENERATED BY INTERNAL SOURCES	3
E. INTERNAL ENERGY CHANGES DURING TRANSIENTS	3
F. HEAT TRANSPORT VIA EMITTED RADIATION	3
G. HEAT TRANSPORT VIA ABSORBED RADIATION	4
H. FORMATION OF DIMENSIONLESS GROUPS	5
II. DESIGN AND FABRICATION OF THERMAL MODELS	12
A. SCALING PROCEDURES	12
B. GENERAL DESCRIPTION	14
C. DESIGN AND FABRICATION	17

TABLE OF CONTENTS (Continued)

	Page
III. TEST EQUIPMENT AND PROCEDURES	37
A. TEST CHAMBER	37
B. TEMPERATURE MEASUREMENTS	37
C. POWER MEASUREMENTS	38
D. TEST PROCEDURES	38
IV. TEST RESULTS	40
A. DESCRIPTION OF TESTS	40
B. PRESENTATION OF DATA	41
V. DISCUSSION	61
A. TEST RESULTS	61
B. UNCERTAINTY ANALYSIS	69
C. PROBLEM AREAS	80
APPENDIX I - CHEMICAL ANALYSIS OF MATERIALS	92
REFERENCES	93

LIST OF TABLES

Table No.		Page
I	Model Dimensions	18
II	Support Wire Heat Leaks	27
III	Summary of Design Heater Power	31
IV	Thermocouple Specifications	36
V	Normal Power Test Results	43
VI	Internal Power Dissipation: Normal Power Tests	46
VII	Double Power Test Results	47
VIII	Internal Power Dissipation: Double Power Tests	50
IX	Three-Dimensional Test Results	51
X	Internal Power Dissipation: Three-Dimensional Tests	54
XI	Comparison of Temperatures: Model 1 - Model 2	55
XII	Comparison of Temperatures: Model 1 - Model 3	58
XIII	Average Box Temperatures	63
XIV	Box Temperature Gradients	66
XV	Simulated Joint Conductance Temperature Gradients: Double Power Tests	68
XVI	Axial Temperature Gradients: Three-Dimensional Tests	70

LIST OF FIGURES

Figure No.		Page
1	Photograph of Thermal Models	84
2	Thermal Model Assembly	85
3	Typical Heater Installation	86
4	Typical Thermocouple Installation	87
5	Thermocouple Locations	88
6	Test Chamber and Instrumentation	89
7	Typical Temperature Distribution: Model 1 - Normal Power	90
8	Correlation of Thermal Model Temperature Data	91

ACKNOWLEDGEMENTS

The authors wish to thank Mr. P. Murphy and Mr. A. Camus for their contributions to assembling and instrumenting the thermal models. Mr. K. Waite was responsible for obtaining the test data.

Dr. J. M. F. Vickers of the Jet Propulsion Laboratory acted as technical monitor for this program. His many helpful suggestions and comments during the course of this work are appreciated.

SUMMARY

Independent dimensionless groups of physical quantities are derived by dimensional analysis to illustrate the possibilities for predicting the temperature distributions in a typical spacecraft from the tests of geometric scale models. This similitude analysis is directed toward spacecraft in which the modes of heat transfer are conduction and radiation. The effects of internal power generation and heat fluxes external to the spacecraft are considered.

Two sets of thermal scaling laws appropriate to spacecraft are discussed. One requires that model and prototype be fabricated from materials having identical thermal properties. In this case, model and prototype differ in temperature at equivalent geometric locations. A second requires that the thermal conductivity of the model differ from that of the prototype. In this case, the temperatures of the model can be made identical to those of the prototype at equivalent geometric locations.

An experimental investigation was carried out to determine the practicability of applying the second set of thermal scaling laws to a typical spacecraft. A prototype, resembling a portion of a JPL spacecraft but somewhat simplified in detail, and two geometric scale models were fabricated in accordance with these laws. One model was approximately one-half scale, the other approximately one-fifth. The temperature distributions in the models and prototype were measured at steady-state conditions in a "space simulation" chamber. Heat fluxes external to the prototype and models, i.e., sunlight, planetary emission, and albedo, were not simulated in these experiments.

Temperature results are presented for tests of models and prototype at two internal power dissipation levels. In these tests, the prototype and models were insulated in order to establish two-dimensional heat flow patterns. Temperature results are also presented for tests in which three-dimensional heat flow patterns were established.

Conclusions and recommendations for additional work, based on the experimental results, are presented.

CONCLUSIONS AND RECOMMENDATIONS

The concept of thermal modeling (where the models are designed to have equivalent temperatures at identical geometric locations) is feasible for certain prototype characteristics. For the prototype configuration used in the experiments described herein, the test results indicated that a half-scale model could be used to predict prototype temperatures to within one percent (3°C) of the absolute temperature level during steady-state operation without external heat flux simulation. Test results for a one-fifth scale model indicated that it could be used to predict average prototype temperatures to within three percent (10°C). We believe that this three percent figure could be reduced considerably by refining the insulation system used on the one-fifth scale model. The magnitude of the errors associated with these tests appear to make the concept feasible for many present generation spacecraft or spacecraft components.

As a result of our investigations of thermal modeling at equivalent temperatures, we also conclude that: (a) the characteristics of the prototype and the type of thermal information required, i.e., average temperatures of components, temperature gradients, etc., will determine the practicability of the concept; and (b) the smallest scaling ratio attainable will be dictated by the prototype characteristics as well as the absolute size of the smallest model. Irrespective of the apparent advantages of building and testing small-scale models, the feasibility of applying the modeling concept to each prototype will have to be studied in advance. Many spacecraft designs will not be amenable to modeling

techniques; nevertheless, it may be possible in certain designs to predict the thermal performance of a flight design more accurately from scale model tests than from tests of prototype size mockups.

In designing thermal scale models of a prototype, it would be valuable to have available a mathematical model of the prototype from which one could assess the influence of uncertainties in variables on the thermal performance. In most spacecraft, the heat flow patterns are sufficiently complex to require a computer solution. From parametric computer studies, it would be possible to design a more accurate model, as these results would indicate regions where details are critical.

During our investigation, we noted several limitations and problem areas pertaining to thermal modeling where equivalent temperatures are preserved in model and prototype. Although the following list is by no means complete, and is derived from the limited number of experiments completed to date, it should serve to give the reader some insight as to the applicability of the concept.

Characteristics of Prototype

(1) Low prototype thermal conductivities will limit the selection of model materials and, therefore, the model scale. If the model conductance is decreased artificially, e.g., by slitting, a detailed analysis will be required to determine the effective conductivity.

(2) Preservation of geometric similitude in models of a small prototype or in one having thin wall sections will limit the scale.

(3) Prototypes which re-radiate small amounts of power per unit area will be difficult to model.

(4) Where temperature gradients are more important to performance than temperature level (for example, differential thermal expansion of optical components), the modeling concept may be limited in usefulness.

Instrumentation

(1) The design of model supports, heater leads, and thermocouple or thermistor leads must be carefully considered to insure that the stray heat leaks from these sources are small with respect to the internal power dissipation of the model.

(2) In models with small internal power dissipations, it may be necessary to resort to infrared temperature measuring techniques to avoid these limitations.

Thermal Control Surfaces

(1) Reproducibility of absorptance for short wavelength incident radiation is difficult, particularly on small models where handling of these surfaces is unavoidable.

(2) Characteristics of thermal control surfaces with low emittances (and therefore high conductivities) will introduce limits on the smallest model which can be scaled, because of the thermal conductance of the coating.

(3) In prototypes with low surface emittances, the uncertainty in temperature may be large, due to the problems of measuring the absolute emittance accurately.

Dimensional Tolerances

(1) May limit the absolute size of smallest scale model.

(2) Particularly important in areas of high emissive power or where large percentages of incident flux are absorbed.

Simulation of Joint Conductances

(1) Thermal model designs must be based on measured or computed joint conductances for the prototype. The detailed design of simulated joints in models may require extensive mathematical analyses when the joints significantly influence temperature distributions.

(2) At present, there are no experimental data to determine whether high or low conductance joints are most difficult to simulate. Further work is required in this area.

Insulations

The use of "super insulations" on many spacecraft prototypes will present difficulties in fabricating small scale models because of the uncertainties inherent in predicting the heat flow through these insulations. Moreover, the effects of "thermal shorts" through seams and penetrations become more significant as the size of the model decreases.

Selection of Model Materials

(1) Where temperature gradients in the prototype are significant, thermal conductivity measurements of the model materials will be required.

(2) For prototypes with very large gradients, some consideration must be given to the variations in material properties with temperature.

We believe that an additional effort is required to accurately predict the thermal performance of a typical spacecraft from tests of thermal scale models. The additional effort should include:

(1) transient performance tests,

(2) a more detailed investigation of the simulation of joint conductance, and

(3) tests with external heat flux simulation.

In addition, the concept of thermal modeling, where model and prototype material properties are preserved, bears further investigation. Although it appears that modeling at equivalent temperatures may alleviate some of the problems associated with property variations with temperature, the alternative approach may be useful in certain prototype designs. An investigation of the limitations of this concept would broaden the understanding of the thermal modeling problem.

INTRODUCTION

The thermal problems associated with the design of spacecraft and certain spacecraft experiments have stimulated interest in methods for predicting the adequacy of thermal control systems. Mathematical analyses, using computers, and full-scale simulation tests of flight hardware (or representations thereof) have been utilized to validate the operation of thermal control systems. As an alternative to the concept of flight testing--which at present does not seem economically justifiable--it may be worthwhile to consider the concept of thermal scale modeling as a tool for predicting the thermal behavior of a spacecraft.

The interest in small-scale model testing is derived from the relatively high costs of space simulation testing with full-scale hardware, and the need for an experimental evaluation of mathematical models (of the thermal characteristics) designed to represent physical configurations. In addition, environmental simulation on a large scale with present "space chambers" may not be precise enough to evaluate certain thermal designs. Small test chambers appear to offer the control and reliability required for precise simulation.

The thermal modeling concept has not been investigated in sufficient detail to adequately define the limitations or the problem areas involved in predicting flight temperatures from scale model thermal testing. The objective of the work described in this report is to examine the practicability of one

approach to thermal scale modeling, and to define certain limitations and problem areas associated with this approach. The experiments performed in this study were based on scaling laws which predict identical temperatures in model and prototype at equivalent geometrical locations. Conclusions and recommendations relating to the practical aspects of applying this thermal scaling technique to a spacecraft are based on the results of the experimental program described herein.

This report summarizes the work performed as Phase II of the subject contract. In the Phase I study, small thermal models of a simple configuration were scaled in accordance with the same laws. Experiments were performed which demonstrated the validity of the scaling laws. The reader is referred to Reference 1 for a summary of the Phase I results.

CORRIGENDA

Report Title: THERMAL SCALE MODELING OF SPACECRAFT: AN EXPERIMENTAL INVESTIGATION

Authors: Fowle, A. A., et al.

Contract: 950252

Date: June 28, 1963

Page 9 The second equation should be corrected to read:

$$\frac{\rho_m C_{pm} L_m^2}{K_m \tau_m} = \frac{\rho_s C_{ps} L_s^2}{K_s \tau_s}$$

Page 9 The ninth equation should be corrected to read:

$$\frac{\rho_m C_{pm} L_m}{\tau_m} = \frac{\rho_s C_{ps} L_s}{\tau_s}$$

I. THE THERMAL MODELING PROBLEM

A. INTRODUCTION

The basis for modeling any physical system must be the derivation of the independent dimensionless groups containing (together) all the physical quantities which interact to determine the behavior of this system. Once having determined the functional relationship between the dimensionless groups, by analysis or experiment, the physical behavior of all similar systems is completely characterized. The advantages of this approach stem from the fact that the independent variables controlling the behavior of the system are reduced to a minimum, and, in cases where experiment is required to determine the behavior, tests at a reduced geometric scale can be used to predict the behavior of a larger system.

The least number of dimensional quantities needed to describe the system and its interaction with its environment must be determined by physical reasoning. This implies, and requires, an understanding of the active physical phenomena.

In the thermal modeling of spacecraft we are concerned with the temperature distributions which result from internal power sources and the thermal interaction of the craft with its environment. Although closed-cycle thermodynamic systems involving flow loops and power machinery may be present in many spacecraft, we confine our attention to spacecraft elements wherein the temperature distributions are determined by heat transfer via the

mechanisms of radiation and conduction in solid members. In order to derive the dimensional quantities which determine the thermal behavior of this class of spacecraft system it is useful to think in terms of the following active heat transfer phenomena:

1. Heat transport by solid conduction
2. Heat transport at solid-to-solid interfaces
3. Heat generated by internal sources
4. Heat (internal energy) changes during transients
5. Heat transport via radiation emitted from surfaces
6. Heat transport via radiation absorbed at surfaces

B. HEAT TRANSPORT BY SOLID CONDUCTION

Heat transport by solid conduction can be characterized by the thermal conductivities of the materials of the system, K, and by the temperature distributions in these materials (which introduces the variable L and T). For a single thermal conductivity value to be sufficient, the materials must be isotropic. If the thermal conductivities of the materials of the system are themselves temperature dependent, then the dimensional quantities which describe this dependence enter.

C. HEAT TRANSPORT AT SOLID-TO-SOLID INTERFACES

Heat transfer at solid-to-solid interfaces, when considered on a macroscopic scale, introduces the concept of thermal resistance or its reciprocal, thermal contact conductance, C. The thermal contact conductance is defined as

the ratio of the heat transfer across the interface per unit of superficial contact area and the temperature difference across the contact gap. It is well known that the value of the thermal contact conductance for systems in vacuo depend on the structural characteristics of the joining materials, on their surface finish, and on the contact pressures.

D. HEAT GENERATED BY INTERNAL SOURCES

In typical spacecraft components, sources of internal heat exist due to the I^2R losses in the electric circuitry. In recognition of these internal sources, it is convenient to introduce a parameter, q^*, which is the internal power generated per unit of volume. The real spacecraft electronic component may be made up of a non-homogeneous mixture of materials, and a practical question will always exist as to the linear scale on which model similarity is to be preserved.

E. INTERNAL ENERGY CHANGES DURING TRANSIENTS

Consideration of the requirements for thermal similitude in non-steady-state systems introduces the thermal inertia properties of the system and the time, τ. The thermal inertia of the system is simply characterized by the product of density (ρ) and specific heat (C_p) of the materials from which it is constituted.

F. HEAT TRANSPORT VIA EMITTED RADIATION

The total emissive power per unit of area of the surfaces making up the system is given by the product of the total hemispherical emittance of the

surface, ϵ, the Stefan-Boltzmann constant, σ, and the fourth power of its absolute temperature. Therefore, consideration of emitted radiation introduces the new factors, ϵ and σ. The total hemispherical emittance, ϵ, is the only factor over which we have experimental control. For any particular surface, ϵ varies with its temperature and surface condition--degree of roughness, oxidation, contamination, etc. In addition, ϵ is a doubly-integrated quantity involving ϵ_λ, the monochromatic emittance, and ϵ_θ, the directional emittance. The latter factors become important only when we consider the intensity and spectral distribution of the radiant flux incident on the surfaces.

G. HEAT TRANSPORT VIA ABSORBED RADIATION

The radiant heat absorbed at a surface per unit area is the product of its absorptance, α, and the incident flux, ϕ. The absorptance depends on the factors affecting emittance (surface temperature, condition and direction) and, in addition, on the characteristics of the incident radiation measured by its distribution in the spectrum. For this reason, it is useful to separate the flux incident on the surface elements of the spacecraft system into components identified by source.

One contribution to the total flux is that which originates within the system, because all exposed surfaces of the system are themselves emitters. The flux from these internal sources falling on any specified surface is a portion of the sum of the reflected and emitted radiation issuing from all the surfaces which the element can "see." This portion depends on the geometry of the system and on the

angular distribution of the radiant energy leaving the "viewed" surfaces. If the intensity of this leaving energy (both emitted and reflected) obeys a known law, such as Lambert's cosine law, then the portion incident can be predicted on the basis of geometry only. The magnitude of the flux issuing from the "viewed" internal sources depends on the emissive power of these surfaces (hence, $\epsilon \sigma T^4$) and the reflected power. The reflected power, in turn, depends on the emissive power of all surfaces, on the geometry, and on the absorptance of all surfaces. In summary, we reason that the absorbed energy depends on the geometry and on the emissive power and absorptance of all surfaces.

The other contributions to the total incident flux are characterized by sources outside the system, for instance, sunlight and reflected or direct radiation from the moon and planets. The influence of each external source must be accounted for by introducing additional variables. ϕ_{o1}, ϕ_{o2}, ϕ_{o3}, etc., which are used to denote the intensity of the radiant energy from the various external sources, and α_{o1}, α_{o2}, α_{o3}, etc., which are used to denote the absorption characteristics of the surfaces of the system to these incident radiations. Of course, an additional requirement for rigorous thermal similitude is that the direction of the radiant flux from external sources is the same in model and prototype.

H. FORMATION OF DIMENSIONLESS GROUPS

From the previous discussion, one notes that the thermal behavior of spacecraft is determined by a very extensive number of dimensional parameters,

and this fact may make thermal modeling for the general case impractical if not impossible. However, the application of certain reasonable restraints can make the problem of thermal modeling tractable.

First, we restrict consideration to model and prototype systems for which the K's, ρ's, C_p's, α's and ϵ's can be considered temperature independent, and, second, to solid materials that can be considered isotropic conductors. Third, to eliminate the influence of the spectral and angular distribution on the emitted and absorbed radiation, we restrict consideration to model and prototype systems which have the same surface characteristics. With these restrictions, a single notation for K, ρ, α, etc., is sufficient for the development of the thermal modeling factors.*

The formation of the controlling dimensionless groups (often referred to as the π groups) may be accomplished in a number of ways. Formal procedures are described in the literature. We prefer a method which points up the physical significance of the π's. Thermal similitude requires that the heat transport and internal energy changes be proportional in model and prototype. To

---

*It is not necessary to include all of these restrictions for every system. Some of these restrictions may be removed. For certain relatively simple thermal systems or components of a total system, some of the restrictions can be removed without making thermal modeling impractical.

state this condition mathematically we proceed as follows. First, we express the heat transfer and energy change effects in dimensional terms:

Effect	Dimensional Statement	
Heat Flux via Solid Conduction	$\frac{KT}{L}$	(watts/cm^2)
Heat Flux at Solid-to-Solid Interface	CT	(watts/cm^2)
Heat Flux Due to Internal Sources	q^*L	(watts/cm^2)
Heat Flux Due to Changing Internal Energy	$\frac{\rho C_p T L}{\tau}$	(watts/cm^2)
Heat Flux via Emitted Radiation	$\epsilon \sigma T^4$	(watts/cm^2)
Heat Flux via Absorbed Radiation (Internal Sources)	$\alpha_T \phi_T$	(watts/cm^2)
Heat Flux via Absorbed Radiation (External Sources)	$\alpha_{o1} \phi_{o1} \alpha_{o2} \phi_{o2}$, etc.	(watts/cm^2)

The ratios of the above expressions with respect to the heat flux due to solid conduction are:

$$\pi_1 = \frac{CL}{K}$$

$$\pi_2 = \frac{q^*L^2}{KT}$$

$$\pi_3 = \frac{\rho C_p L^2}{K\tau}$$

$$\pi_4 = \frac{\epsilon \sigma T^3 L}{K}$$

$$\pi_5 = \frac{\alpha_T \phi_T L}{KT}$$

$$\pi_6, \pi_7, \text{ etc.} = \frac{\alpha_{o1} \phi_{o1} L}{KT} \quad , \quad \frac{\alpha_{o2} \phi_{o2} L}{KT}, \text{ etc.}$$

As the temperature, T, appears in a number of the above-listed π's, and as temperature can be considered a dependent variable in the experimental model studies, a more convenient set can be gained by rearrangement as follows:

$$\pi_1 = \frac{CL}{K}$$

$$\pi_2 = \frac{q^* L^2}{KT}$$

$$\pi_3 = \frac{\rho C_p L^2}{K\tau}$$

$$\pi_4 = \frac{\varepsilon \sigma q^{*3} L^7}{K^4}$$

$$\pi_5 = \frac{\alpha_T \phi_T}{\varepsilon \sigma T^4}$$

$$\pi_6, \pi_7, \text{ etc.} = \frac{\alpha_{o1} \phi_{o1}}{q^* L} \quad , \quad \frac{\alpha_{o2} \phi_{o2}}{q^* L}$$

A useful set of scaling laws for model testing would specify that the temperature-time distributions in normalized space would be identical in model and prototype. In addition, we have the restriction that the emittance and absorptance of corresponding surfaces in model and prototype are identical. In this instance, for thermal similitude

$$\frac{C_m L_m}{K_m} = \frac{C_s L_s}{K_s}$$

$$\frac{q^*_m L^2_m}{K_m} = \frac{q^*_s L^2_s}{K_s}$$

$$\frac{\rho_m C_{pm} L^2_m}{K_m} = \frac{\rho_s C_{ps} L^2_s}{K_s}$$

$$\frac{q^{*3}_m L^7_m}{K^4_m} = \frac{q^{*3}_s L^7_s}{K^4_s}$$

$$\pi_{5m} = \pi_{5s} \text{ (identically satisfied)}$$

$$\frac{\phi_{o1m}}{q^*_m L_m}, \frac{\phi_{o2m}}{q^*_m L_m}, \text{ etc.} = \frac{\phi_{o1s}}{q^*_s L_s}, \frac{\phi_{o2s}}{q^*_s L_s}, \text{ etc.}$$

$$\frac{L_m}{K_m} = \frac{L_s}{K_s}$$

$$C_m = C_s$$

$$q^*_m L_m = q^*_s L_s$$

$$\rho_m C_{pm} L_m = \rho_s C_{ps} L_s$$

$$\phi_{o1m}, \phi_{o2m}, \text{ etc.} = \phi_{o1s}, \phi_{o2s}, \text{ etc.}$$

It is this last set of scaling laws which we have examined experimentally in the subject contract. As these experiments were made at steady state, the thermal inertia characteristics of the models do not enter the problem. In addition, ϕ_{o1}, ϕ_{o2}, etc., were made negligible in the design of the experimental apparatus. In summary, we would predict the same temperature at corresponding points if

$$\frac{L_m}{K_m} = \frac{L_s}{K_s}$$

$$C_m = C_s$$

$$q^*_m L_m = q^*_s L_s$$

Other possibilities certainly exist and deserve attention. For instance, suppose it is convenient to make the model and prototype of identical materials. Suppose further, we place the additional restriction that the radiation characteristics of corresponding surfaces in model and prototype are identical. Then, in this case,

$$C_m L_m = C_s L_s$$

$$\frac{L^2_m}{\tau_m} = \frac{L^2_s}{\tau_s}$$

$$q^*_m L^{7/3}_m = q^*_s L^{7/3}_s$$

$$T_m L^{1/3}_m = T_s L^{1/3}_s$$

$$\pi_{5\,m} = \pi_{5\,s}$$

$$\phi_{01\,m} L^{4/3}_m, \phi_{02\,m} L^{4/3}_m, \text{ etc.} = \phi_{01\,s} L^{4/3}_s, \phi_{02\,s} L^{4/3}_s, \text{ etc.}$$

The above laws, of course, hold only when the properties of the model and prototype are independent of temperature.

II. DESIGN AND FABRICATION OF THERMAL MODELS

A. SCALING PROCEDURES

In the following section we will describe the physical characteristics of three thermal models designed in accordance with the set of scaling laws which would specify that the temperatures be identical at equivalent geometrical locations in the models. We chose to make the surface characteristics, emittances, of model and prototype identical, and to make the tests at steady-state conditions. In addition, the heat flux incident on the models was made negligible in the design of the experimental apparatus. For this situation we would predict identical temperatures at equivalent geometrical locations when

$$\frac{L_m}{K_m} = \frac{L_s}{K_s}$$

$$C_m = C_s$$

$$q^*_m L_m = q^* L_s$$

Three models were fabricated and tested in accordance with the above set of scaling laws, by using different materials of construction and internal power dissipations in each model.

The largest model (prototype), referred to as Model 1, was designed to fit conveniently in our space simulation chamber, and was fabricated from Armco iron, a relatively pure iron used as a thermal conductivity standard. Model 2 was fabricated from SAE 4130 steel, which has a thermal conductivity

approximately half that of Armco iron. The smallest model, Model 3, was fabricated from 304 stainless steel, which has a thermal conductivity approximately one-fifth that of Armco iron.

The following conductivities were established from literature data for each of the materials (where the subscripts refer to the model):

$K_1 = 0.730$ (Armco iron at 70°F, Ref. 2)

$K_2 = 0.410$ (SAE 4130 at 70°F, Ref. 3)

$K_3 = 0.156$ (304 S.S. at 70°F, Ref. 3)

From these values the appropriate characteristic length ratios are calculated to be

$$\frac{L_1}{L_2} = 1.7805$$

$$\frac{L_1}{L_3} = 4.679$$

Thus, all linear dimensions of Model 1 (the prototype) were 1.7805 times as large as those of Model 2 and 4.679 times as large as those of Model 3. (It should be noted that the thermal conductivity of samples of the actual materials of construction used in these thermal models is being determined experimentally at three temperature levels as a check on the design values obtained from literature data. The results of this work were not available at the time this report was written.)

The simulated joint conductances of each model were made identical to satisfy the second relationship which states that

$$C_1 = C_2 = C_3$$

The details of the construction of the simulated joints are described in more detail in Section II-C2.

The internal power dissipation in each model was scaled in accordance with the third relationship, which can be rearranged to give:

$$\frac{P_1}{L_1^2} = \frac{P_2}{L_2^2} = \frac{P_3}{L_3^2}$$

where:

P = internal power dissipation (watts)

L = characteristic length

We find that

$$\frac{P_1}{P_2} = 3.1702$$

$$\frac{P_1}{P_3} = 21.893$$

In summary, we chose the over-all dimensions of Model 1 (the prototype in this case) to be the largest model size which would conveniently fit in our test chamber. Models 2 and 3 were scaled from Model 1 using the scaling ratios.

In the following sections, we will describe the design and fabrication of the thermal models in detail.

B. GENERAL DESCRIPTION

The basic configuration of the thermal models was chosen to represent the elements of a portion of a typical JPL spacecraft. It was not desired to duplicate the details of a JPL spacecraft, but rather to simulate the typical heat flow patterns with models which could be easily fabricated and tested.

Several "ground rules" pertaining to the design of the models were established by JPL in our Statement of Work. The models were to be designed in conformance with the following general concepts:

(1) Maintain an average model temperature at or near room temperature at normal power conditions.

(2) Provide for nonuniform internal power dissipations within a given model. To simulate electronics packages, several boxes dissipating internal power were required. It was desired to design one box to dissipate five times as much total power as the box with the lowest power dissipation. Within a given box it was desired to have two heaters, one dissipating approximately twice as much power as the other.

(3) Fabricate the boxes on a given model with differing wall thicknesses. One box was to have twice the wall thickness of the others.

(4) Design a basic configuration which could be insulated to provide for either a two- or three-dimensional heat flow pattern within the model.

(5) Provide a method for attaching the boxes to the frame members through thermal resistances to simulate a joint resistance.

To simulate the electronics packages in a typical spacecraft, three "boxes", each containing internal electrical power sources, were arranged in a triangular fashion around a cylindrical tube which represented the walls of a mid-course guidance motor. A photograph of the three models showing the relative sizes and the arrangement of the boxes is shown in Figure 1.

The boxes and the simulated mid-course guidance motor were supported by three vertical angles which formed a frame. The individual boxes were attached to the frame with support tabs which were designed to simulate a typical joint conductance. The simulated mid-course guidance motor was also supported from the frame by six thin struts. The top and bottom of the model was insulated with NRC-2[(1)] insulation to establish a two-dimensional heat flow pattern within the model. (One insulation package, however, was made removable so that in certain tests we could establish end-to-end gradients.) The faces of each box were coated to have different average emittances and thereby control the heat flow patterns.

A drawing illustrating the over-all configuration and certain of the details is presented in Figure 2.

---

(1) National Research Corporation, Cambridge, Mass.

C. DESIGN AND FABRICATION

1. Fabrication and Assembly of Components

The three boxes (c.f. Figure 2) used in Models 1 and 2 were fabricated by welding the sides and the two vertical dividers to the outward facing wall. Full penetration welds were made using a filler rod of the same material as the boxes. After welding, the exterior surfaces of the boxes were surface-ground to the proper dimensions. The boxes for Model 3 were fabricated from a single sheet of material and formed in a precision jig. The corners and the dividers were heli-arc welded. Table I lists the pertinent dimensions for the boxes of the three models.

As shown in Figure 2, the vertical dividers supported the radiation shields. The shields were attached to two tabs with soft solder after the heaters and thermocouples had been installed. A small gap around the periphery of the shields prevented heat from flowing conductively between the shields and the boxes. The ends of the vertical dividers were separated from the boxes in such a way that the main heat flow paths (by conduction) were through the box faces.

Three vertical angle frames supported the boxes and the simulated mid-course guidance motor. The frames on Models 1 and 2 were fabricated from two pieces welded (with full penetration welds) along a corner. The frames for Model 3 were fabricated by bending a single piece to the proper angle.

Milled slots at the top and bottom of each frame were used to position the "simulated joint conductance" tabs. These tabs were made as an integral part

TABLE I

MODEL DIMENSIONS

	Model 1	Model 2	Model 3
Boxes (in.)			
Length	18-61/64	10-21/32	4.048
Width	15-27/64	8-41/64	3.286
Depth	2-1/2	1-13/32	0.534
Wall Thickness			
Boxes A & B	0.292	0.164	0.062
Box C	0.146	0.082	0.031
Joint Conductance Tabs (in.)			
Width	1.497	0.843	0.320
Thickness			
Boxes A & B	0.292	0.164	0.062
Box C	0.146	0.082	0.031
Length	0.182	0.102	0.039
Frame Thickness (in.)	0.292	0.164	0.062
Measured Gap Areas ($in.^2$)			
Frame I	3.106	0.892	0.168
Frame II	2.756	0.861	0.214
Frame III	2.567	0.924	0.162

of the box, i.e., the top and bottom were milled out to the shape shown in Figure 2. The step in the tab was used to position the box with relation to the frame. Note that the smallest part of the tab penetrated through a milled slot in the frame.

This protrusion was welded to the frame with a full penetration weld. In this manner the boxes were separated from the frame by members of known cross-sectional areas and lengths. Any heat flowing from box to box by conduction was thus required to flow through these standoffs. A fuller discussion of these simulated joint conductances is given in the following section.

The thin-walled mid-course guidance motor was supported from the frames by six members of small cross-sectional area. The support members were welded in slots on the motor and the frame.

All three models were assembled in the same basic manner. After welding the dividers to the boxes, Boxes B and C were gold plated (c.f. Section II-C3). The heaters and thermocouples were installed on the interior of the boxes and the entire inner surface painted with an optical black paint. The radiation shields were soldered to the dividers (with attached thermocouples) and also painted black. The mid-course guidance motor and frames (with thermocouples) were assembled as a unit and then painted black. The next assembly consisted of welding the boxes to the frame at the joint conductance tabs. To preclude damage to the gold surfaces by heating, the boxes were placed in a shallow pan of water before the tabs were welded to the frame. Particular care was taken to insure that the gaps between the corners of the boxes were the correct dimension. We

found this to be the most difficult part of the assembly, and we were not completely successful in maintaining the correct tolerance on this dimension. In Table I we have listed the gap dimensions as measured after assembly. It should be noted that inaccuracies in these dimensions affect the thermal performance of the model. The significance of these errors are discussed in detail in the "Discussion of Results."

The next steps in the assembly were to attach the thermocouples to the tabs and apply the proper amount of optical black paint to the external surfaces of Boxes B and C, as shown in Figure 2. All of the heater leads and thermocouples were brought out from the model through the gaps between the boxes.

The insulation packages were assembled separately and attached to the top and bottom of the model by cementing. The details of this installation are shown in Figure 2.

The final assembly was the attachment of the three support wires to the model. During the assembly, particular care was taken to avoid handling the thermal control surfaces on the boxes.

2. Simulated Joint Conductances

The design of the stand-offs used to simulate the joint conductances was quite arbitrary. The basic reason for using the construction shown in Figure 2 was to have a reproducible resistance between the frames and the boxes in each of the models. The choice of the configuration used in Model 1 (prototype) was, therefore, predicated on a design which would be simple to reproduce in the smaller

models. This is not, of course, the problem which would be encountered if it were necessary to design a simulated joint of a prescribed conductance.

If we assume that the heat flow through the tab is approximately one-dimensional, the equivalent conductance is

$$C = \frac{k}{\ell}$$

where:

C = conductance (watts/cm^2 °K)

k = thermal conductivity (watts/cm °K)

ℓ = length of tab between the frame and box (cm)

From the scaling laws, we know that for temperature similarity the following relation must be satisfied:

$$C_1 = C_2 = C_3$$

or

$$\frac{k_1}{\ell_1} = \frac{k_2}{\ell_2} = \frac{k_3}{\ell_3}$$

Since the conductivity of the tab was identical to that of the model and since all lengths were scaled in accordance with the second relation, we satisfied the condition that the joint conductances were identical from model to model.

For Box A of Model 1, the heat flow for four tabs (1.497 x 0.292 x 0.182 inches long) of Armco iron is approximately 17.8 watts per degree of temperature difference between the box and the frame. (This estimate is based on a one-dimensional model.)

If we now consider that a typical spacecraft electronics package is attached to a frame through a flanged joint, the heat flow through the joint is

$$q = C_j A_j \Delta T$$

where:

C_j = mean joint conductance (watts/cm^2 °K)

A_j = joint area (cm^2)

ΔT = temperature difference between flange and frame (°K)

Thus, with the tabs, we are simulating a case where

$$C_j A_j = 17.8 \text{ watts/°K}$$

For a typical electronics package of the same approximate dimensions as the boxes on Model 1, we estimate that the total flange area might be approximately 350 cm^2. Thus, the mean value of the joint conductance being simulated is

$$C_j = 0.05 \text{ watts/cm}^2 \text{ °K}$$

Joint conductances of this magnitude are representative measured values for loaded metal-to-metal joints in vacuo.

It should be noted that the four tabs on Boxes A and B were of similar dimensions, whereas the tabs on Box C were half as thick. The mean value of the joint conductance in Box C would thus be half the above value.

We should re-emphasize that this approach to the design of a simulated joint will not, in general, be adequate where it is desired to fabricate a simulated joint of a given conductance.

3. Thermal Control Surfaces

The choice of the properties of the thermal control surfaces was based on the requirement that one box of a model would have a total internal power dissipation approximately five times that of the lowest power box, with the third box intermediate. In addition, it was desired to maintain the average temperature of each box at or near room temperature for "normal power" tests.

To accomplish this objective, we coated the entire box which dissipates the largest amount of power with an optical black paint.[1] The interior of each box as well as the frames, mid-course guidance motor, and radiation shields were also coated with the same paint. We measured the total hemispherical emittance of this particular paint in our laboratory and found it to be 0.97 ± 0.05 at room temperature.

Since the other two boxes dissipated less power, it was necessary to adjust their average surface emittance so that each box would have approximately the same temperature. To accomplish this objective, the outward-facing surfaces of these two boxes were first coated with a gold surface having a low emittance. A fraction of this surface was then painted with the high emittance, optical black paint to obtain the desired average emittance.

---

(1) Minnesota Mining & Manufacturing Co., St. Paul, Minnesota (3M Brand Velvet Coating, Series 9560).

A gold surface was chosen, because it has a high reflectance and the surface characteristics are reproducible. A copper and a silver "flash" were deposited before the final gold deposition. To obtain a highly reflective surface and a reproducible finish, the boxes were surface-ground and buffed before a deposition; the surfaces were buffed after each deposition. The following plating thicknesses were used on all surfaces:

Copper	0.00045 inch
Silver	0.00072 inch
Gold	0.00010 inch

Samples of gold-surfaced Armco iron, SAE 4130, and 304 SS were fabricated and the emittances measured by Jet Propulsion Laboratory. The results indicated that each of the samples had an emittance of 0.04 ± 0.005. No noticeable difference between samples was observed.

The details of the "black" striping on the box faces are shown in Figure 2. To satisfy the scaling law which requires that the emittances from model to model be equivalent, the ratio of black to gold area was made identical on each model. In the following tabulation, we have listed the nominal dimensions for the areas of gold and black on each box of Model 1. The average emittance was calculated by assuming that $\epsilon = 0.97$ for the black surfaces and 0.04 for the gold surfaces.

	Box A	Box B	Box C
Total exposed area ($in.^2$)	387.06	387.06	387.06
"Black" area, $\epsilon = 0.97$ ($in.^2$)	387.06	144.81	63.97
Average emittance	0.97	0.388	0.194

It should be noted that the effective emittance of these boxes calculated from the total surface area of the boxes is not exact, since the triangular box arrangement produces reflections at the corners of the boxes. However, for purposes of modeling it is only necessary to insure that the model and prototype have identical emittances at equivalent geometrical locations.

In applying the black paint striping to Boxes B and C, it was necessary to maintain a close tolerance on the area, since the model temperatures were extremely sensitive to this parameter. We estimate that the width and height of the black areas on Boxes B and C were accurate to within $\pm$ 1/64 inch. The largest uncertainties are prevalent in Box C of Model 3. In this case, the error in the black area was approximately $\pm$ 5% for a $\pm$ 1/64 inch tolerance.

4. Model Supports

The thermal models were supported by three, small diameter stainless steel wires attached to the LN_2 shroud in the test chamber. Since the support wires constitute a heat leak from the model, it was necessary to scale the wire sizes such that the ratio of the support wire heat leak to the total power dissipated is essentially constant for all models.

In our test setup, the temperature distribution in the wires was dominated by the radiative heat leak to the LN_2 wall. In this case, it can be shown that the heat leak is given by the expression

$$q_w = \sqrt{2/5\ k\ A_c\ P\ \epsilon\ \sigma T_o^5}$$

q_w = wire heat leak

k = thermal conductivity

A_c = cross-sectional area of wire

P = perimeter

ϵ = surface emittance

T_o = model temperature

For similar support wire materials

$$q_w \alpha D^{3/2}\ T_o^{5/2}$$

From the scaling ratios for these models, we would have exactly scaled heat leaks from model to model if

$$\frac{q_{w1}}{q_{w2}} = 3.1702$$

$$\frac{q_{w1}}{q_{w3}} = 21.893$$

where the subscripts refer to the model.

Since the models were designed to have identical temperatures,

$$\frac{D_{w1}}{D_{w2}} = 2.155$$

and

$$\frac{D_{w1}}{D_{w3}} = 7.81$$

In the practical case, one cannot always choose wire diameters necessary for exact scaling; however, if the support heat leak is small with respect to the total power dissipated by the model, the temperature errors will be small. Table II lists the wire diameters, etc., and the ratio of the total support wire heat leak to the total power dissipated in the model.

TABLE II

SUPPORT WIRE HEAT LEAKS

	Model 1	Model 2	Model 3
Support Wire Diameter (inches)	0.0625	0.030	0.010
Support Wire Material	S.S.	S.S.	S.S.
Actual ratio of wire diameter $\left(\frac{D_{w1}}{D}\right)$	1	2.08	6.25
Correct ratio of wire diameter $\left(\frac{D_{w1}}{D}\right)$	1	2.155	7.81
Number of support wires	3	3	3
Support wire heat leak (percentage of total model power dissipation)	0.16	0.17	0.23

From Table II it can be seen that the support wire heat leaks are a small percentage of the total power dissipation and that small errors in the scaling of the wires will therefore not appreciably affect the model temperatures.

5. Insulation

The insulation packages were designed to prevent heat from flowing out of the ends of the models. The location and the details of the assembly are shown in Figure 2.

The insulation was fabricated as a package using crinkled aluminized Mylar foils[1] mounted on a pad of polyurethane foam. The foam pads were cut to a triangular shape which fit on the ends of the model. The foam was 1/2-inch thick on Model 1. Sixty layers of NRC-2 were crinkled and placed loosely on the foam. The total thickness was approximately 1-1/4 inches. Six of the layers were folded over the edges of the package, and the outermost foil was folded under the foam pad and sewed to the foam. This outermost wrap was thermally short-circuited to the model. However, we felt that the additional heat leak along the foil would be less than that which would occur if a small gap were left between the model and the foils.

Each model was insulated in the same manner. However, in the smallest model it was difficult to make the layers "fluffy", i.e., they were somewhat compressed. This compression is deleterious to the effectiveness of the insulation,

---

(1) NRC-2, product of National Research Corporation, Cambridge, Mass.

and we expect that the heat flux was higher in this small model. In addition, the edges were more difficult to fold, thus compressing the foils. This situation increases the strength of the "thermal edge short".

An accurate calculation of the magnitude of the heat leak through these insulation packages cannot be made when one considers these edge effects. We can, however, estimate the magnitude of the heat leak as if the heat flow were one-dimensional. Thermal conductivity tests in our laboratory on these insulations (work not performed under this contract) indicate that a typical thermal conductivity at 120 layers/inch, between the temperature limits of 300 and 77°K, is approximately 6×10^{-6} watts/cm °K. For a thickness of approximately 1.5 cm, the total heat leak from Model 1, is estimated to be 2.2 watts through two insulation packages having an area of approximately 4000 cm^2. This is approximately 1.3 percent of the total power dissipated.

The above calculation underestimates the actual heat leak, because of the edge losses, and we would estimate that the heat leak might be several times the above amount. Furthermore, we would expect the percentage heat loss to increase as the size of the package is decreased, because of the increasing importance of the edges.

6. Instrumentation

a. Heaters

As shown in Figure 3, the heater elements were bonded to the two vertical dividers in each box. Two separate heaters were bonded to each divider so

that we could provide current to either or both heater elements on a given divider. In model tests at normal power, current was supplied to only one heater on each divider. For double power tests, current was supplied to both heater elements on each divider.

The heaters[1] were made from Evanohm[2] resistance wire insulated by silicone rubber and fiberglass cloth. The Evanohm wire was selected because of its low temperature coefficient of resistance and because it would minimize resistance changes with temperature. All of the heaters were designed to maintain a uniform watt density over the heater area. The heater elements were bonded to the dividers with Silastic[3] adhesive under pressure and allowed to cure for 12 hours. After installation, the resistance of each heater element was measured accurately at room temperature using a wheatstone bridge.

Table III lists the nominal design heater power specifications for each box of each model. (The reader is referred to Figure 2 for the locations of the boxes and dividers.)

To supply current to the heater elements, twelve heater leads were connected to the model from a hermetic seal on the chamber. Since these wires were exposed and could radiate to the LN_2 temperature shrouds, it was necessary

---

(1) Electroflex, Inc., Hartford, Conn.

(2) W. B. Driver Co., Newark, N. J.

(3) Dow Corning Corp., Midland, Michigan

TABLE III

SUMMARY OF DESIGN HEATER POWER
(watts)

		Model 1	Model 2	Model 3
Box A				
	Divider A	69.2	21.8	3.16
	Divider B	34.6	10.9	1.58
	Total	103.8	32.7	4.74
Box B				
	Divider A	27.7	8.74	1.265
	Divider B	13.8	4.35	0.630
	Total	41.5	13.09	1.895
Box C				
	Divider A	13.8	4.35	0.630
	Divider B	6.9	2.18	0.315
	Total	20.7	6.53	0.945
TOTAL MODEL POWER		166.0	52.32	7.58

to design the heater leads so as to minimize the heat leak to or from the model. In our case it was possible to do this by choosing the proper heater lead materials and sizes.

If the lead wire is in thermal equilibrium with a low temperature sink (and the wire is long), the temperature in the wire can be made uniform by proper choice of the current, wire size, and wire material. If the temperature is made uniform and equal to the model temperature, the gradient at the model, and therefore the heat leak, will be zero. A heat balance on a length element of wire yields the expression

$$I^2 \rho = \pi D_w \epsilon_w \sigma T^4$$

where:

I = current (amps)

ρ = wire resistivity (ohms/cm)

D_w = wire outside diameter (cm)

ϵ_w = wire emittance

T = wire temperature (°K)

The current was fixed by the power dissipation required in the heaters, and the temperature was chosen to be the design temperature of the model. We then chose a wire material and diameter which would minimize the heat leak. (An emittance of 0.8 was assumed for a varnish insulation.)

The following tabulation lists the materials and wire sizes chosen for the heater lead wires on each model.

	Model 1	Model 2	Model 3
Wire material	Manganin	Manganin	Tophet C[1]
Wire size	#32	#38	#38

It should be noted that these wire sizes do not exactly satisfy the "no heat leak" situation. However, we have estimated that, if no current were supplied the total heat leak from the lead wires would be only 0.04% of the total power supplied to Model 1 and 0.3% of that supplied to Model 3. This is due to the relatively low thermal conductivity of the lead wires.

b. Thermocouples

Forty-eight copper-constantan thermocouples were attached to each model. The couples were welded and calibrated against four precision thermometers at four different temperature levels between 0 and 50°C. The over-all accuracy of the thermocouple measurements was within $\pm$ 1/4°C. After calibration, the thermocouples were soft soldered to each model. A short length of lead wire was coiled and attached to the surface with copper cement. A view of a typical installation prior to cementing is shown in Figure 4.

The locations of the 48 thermocouples on a model are shown in Figure 5. Three thermocouples were attached to the inside of each box face at the centerline. Temperatures were also measured at each simulated joint conductance tab, at the top and bottom of each frame, at three centerline locations on the mid-course

(1) W. B. Driver Company, Newark, N.J.

guidance motor and at each radiation shield. It should be noted that the thermocouple locations as noted in Figure 5 were identical in all three models. The numbering system was also identical.

In order to minimize the errors associated with heat leaks along the thermocouple wires, the leads were scaled in accordance with the thermal scaling laws. The scaling laws are satisfied when

$$\frac{q_1}{q_2} = 3.1702$$

and

$$\frac{q_1}{q_3} = 21.893$$

In the three thermal models, we treated the thermocouple heat losses as scaled parameters and attempted to choose the proper wire configuration such that the heat losses obeyed the above relations.

For "long" thermocouples radiating to a low temperature sink from a fixed end temperature, it can be shown (c.f. Reference 1) that the heat leak along the wire is given by

$$q_o = 2/5\ k\ A_c\ P\ \epsilon\ \sigma\ T_o^5$$

where:

q_o - heat flow

k - thermal conductivity

A_c - cross-sectional area

P - perimeter

ε - emittance

T_o - temperature

When the thickness of the insulation is not very large with respect to the wire diameter and the wires have a high conductivity, the area is based on the wire diameter and the perimeter on the outer diameter of the insulation.

By assuming that the surface emittances were identical, and since the model temperatures were designed to be equal, we can express the heat leak relation (for a given number of wires of the same material) as

$$\frac{q_1}{q_2} = C \frac{(D_W D_i^{1/2})_1}{(D_W D_i^{1/2})_2}$$

where:

C = constant

q = heat leak

D_W = wire diameter

D_i = insulation outer diameter

and the subscripts refer to the model number.

Thus, by choosing wire diameters we were able to approximately scale the heat leaks. It should be noted that because the total thermocouple heat leaks were a small percentage of the total dissipated power, errors in this scaling did not affect the model temperatures significantly.

In modeling an actual spacecraft, however, it will be necessary to make the heat leaks through the instrumentation a very small percentage of the total power.

In Table IV we have tabulated the details of the thermocouples and the ratio of the lead heat leak to the model power dissipation.

TABLE IV

THERMOCOUPLE SPECIFICATIONS

	Model 1	Model 2	Model 3
Wire material	Cu-Const.	Cu-Const.	Cu-Const.
Wire size	#30	#36	#40
Wire diameter (in.)	0.010	0.0050	0.0031
Correct ratio of heat leak $\left(\frac{q_1}{q}\right)$	1.0	3.1702	21.893
Actual ratio of heat leak $\left(\frac{q_1}{q}\right)$	1.0	2.2	20.65
Heat leak (percentage of total internal power dissipation)	3.97	5.72	4.2

III. TEST EQUIPMENT AND PROCEDURES

A. TEST CHAMBER

The "space simulation" chamber used in the thermal modeling experiments had an internal diameter of 32 inches and a length of 30 inches. An interior shroud was maintained at approximately 77°K by circulating liquid nitrogen through coolant passages in the shroud. The shroud was made of stainless steel and the surface was coated with "3-M" optical black paint to produce a high emittance finish.

A ten-inch diffusion pump was used to evacuate the chamber. The pressure within the chamber was measured by several thermocouple gages. At low pressures, an ion gage was used. During the test program we were able to maintain the internal pressure at or below 10^{-7} torr (with the shroud cooled to 77°K) with the largest test model. The pump-down time was approximately 3 to 4 hours.

A schematic view of the chamber and the instrumentation is shown in Figure 6.

B. TEMPERATURE MEASUREMENTS

The test model temperatures were obtained by amplifying the thermocouple voltages with a precision amplifier having a gain of 1000 to 1 and displaying the signal on a digital voltmeter. The thermocouples were referenced to a 0°C cold junction. A standard cell was used to periodically check the operation of the amplifier and the digital voltmeter. The temperatures at the 48 model locations were read out in succession by use of a 48-channel selector switch.

C. POWER MEASUREMENTS

The heaters were supplied with current by individual voltage-regulated power supplies. In order to compute the heater powers, the circuit currents were measured by obtaining the voltage drops across precision shunts ($\pm 0.1\%$). The resistances of the heaters were measured accurately before installation of the heater lead wires and external circuitry. The heater powers were then obtained by computing the I^2R loss in the heaters themselves.

An uncertainty analysis of the measurements was completed to determine the most probable error. By considering the heater resistance changes with temperature, the accuracy of the shunts, and the accuracy of the measuring equipment, we estimated that the most probable error in power measurements was less than $\pm 0.7\%$.

D. TEST PROCEDURES

After the models were installed in the chamber, the system was pumped down, and liquid nitrogen was circulated through the thermal shroud. The input power to each heater was adjusted to the desired value with the power supply controls. The models were then allowed to come to thermal equilibrium. The temperatures in Models 1 and 2 were recorded at two hour intervals, together with the input powers, until the models nearly reached equilibrium. At this point, measurements were made at one-hour intervals. Data for Model 3 was recorded at one-hour intervals.

The final "steady-state" readings were taken when the temperatures at several successive intervals did not change by more than approximately 0.1°C. The average time required to complete each test was 27, 14 and 8 hours for Models 1, 2, and 3, respectively. During the tests, the pressure within the vacuum chamber was maintained below 10^{-6} torr to eliminate gas conduction effects.

IV. TEST RESULTS

A. DESCRIPTION OF TESTS

In this section, we present the experimental data obtained for each of the three thermal models. The measured equilibrium temperatures for each test are identified by a location number. (For the thermocouple locations for the models, see Figure 5.) The measured input powers for each test are also tabulated. The reader is referred to Figure 2 for the box and divider locations.

Three separate tests were made with each model. The first set involved testing each model at normal power conditions. The input powers to Model 1 were adjusted to approximately the design values which would produce an average model temperature of 30°C. In these tests, both ends of the models were insulated to minimize longitudinal temperature gradients. Once the measured input powers for Model 1 were established, the appropriate input powers for Models 2 and 3 were obtained from the scaling ratios. The tests of Models 2 and 3, for this normal power condition, were then made by adjusting the input powers to the proper scaled value.

The second set of tests was completed at approximately double power with the same configurations, i.e., insulated models. The appropriate input powers for Models 2 and 3 were again obtained from the measured values for Model 1.

The third set of tests was completed with the insulation package removed from the top of the models. The bottom insulation package was retained. To minimize the area of high emittance surface viewing the LN_2 temperature wall, the end of the mid-course guidance motor was partially insulated by a single circular sheet of NRC-2 insulation attached to the periphery of the motor. The same procedure was followed for all three models. By removing the insulation package, the tops of the boxes and fractions of the radiation shields, frames, and mid-course guidance motor were allowed to view the low temperature sink. In the test, the input powers to Model 1 were adjusted to produce an average model temperature of approximately 30°C. The appropriate input powers for Models 2 and 3 were then scaled from these values. In these tests, the removal of the insulation set up longitudinal gradients in the model; these tests are referred to as "three-dimentional tests."

In addition to these nine tests, a single test using Model 1 was completed to determine whether the three boxes were radiatively coupled. In this test, a shield of low emittance (5-mil aluminum) was placed between each of the boxes and the mid-course guidance motor, thus decreasing the effective radiative couplings between boxes. The insulation packages were replaced on the ends of the model. This test was not repeated for Models 2 and 3.

B. PRESENTATION OF DATA

In Tables V, VII, and IX we have tabulated the temperatures of the three models at identical geometric locations for the normal power, double power, and

three-dimensional tests. The temperatures are measured in degrees Centigrade, and the locations are referenced to Figure 5. The input powers to the heaters for these tests are tabulated in Tables VI, VIII and X. The locations of the heaters and the arrangement of boxes is presented in Figure 2.

Comparisons of the measured temperatures at identical geometric locations for the models are presented in Tables XI and XII. In both tables, we have referenced the comparisons to the temperatures measured for Model 1, for the normal power, double power, and three-dimensional tests.

A discussion of these test results is presented in Section V.

TABLE V

NORMAL POWER TEST RESULTS
(models insulated on top and bottom)

T.C. No.	Location	Temperatures (°C) Model 1	Model 2	Model 3
1	Box A Face	36.48	36.52	34.49
2	Box A Face	30.10	32.83	28.51
3	Box A Face	26.71	27.66	23.80
4	Box C Face	26.17	27.15	21.02
5	Box C Face	35.31	34.54	24.68
6	Box C Face	41.67	38.98	27.34
7	Box B Face	40.48	38.48	27.10
8	Box B Face	31.79	32.05	22.80
9	Box B Face	26.00	26.61	20.58
10	Frame I Bottom	30.51	29.85	23.44
11	Frame I Top	30.27	29.88	25.35
12	Frame II Top	25.95	26.41	21.73
13	Frame II Bottom	26.27	26.85	20.80
14	Frame III Top	36.83	35.43	25.20
15	Frame III Bottom	37.29	35.00	24.49
16	Frame I Top	29.90	29.76	24.00
17	Frame I Bottom	29.98	29.68	22.80

TABLE V (Continued)

T.C. No.	Location	Temperatures (°C) Model 1	Model 2	Model 3
18	Frame II Bottom	26.54	27.12	20.65
19	Frame II Top	26.12	26.46	21.00
20	Frame III Top	36.40	35.10	25.38
21	Frame III Bottom	36.83	34.85	24.27
22	Box C Top	29.15	29.02	22.65
23	Box C Bottom	29.02	28.73	21.59
24	Box C Bottom	37.46	34.93	24.51
25	Box C Top	37.17	35.71	25.10
26	Box B Top	35.98	34.78	25.12
27	Box B Bottom	36.64	34.66	24.07
28	Box B Top	25.75	26.49	20.88
29	Box B Bottom	26.59	26.85	20.33
30	Box A Top	25.22	25.38	21.15
31	Box A Bottom	25.55	25.50	20.15
32	Box A Top	30.20	29.76	25.92
33	Box A Bottom	30.46	29.27	23.63
34	Shield Box A Out	38.88	38.33	34.41
35	Shield Box A In	37.85	38.14	33.86
36	Shield Box A In	31.02	31.83	27.27
37	Shield Box A Out	30.34	30.88	26.71

TABLE V (Continued)

T.C. No.	Location	Temperatures (°C) Model 1	Model 2	Model 3
38	Shield Box B Out	28.49	29.02	22.18
39	Shield Box B In	38.17	36.81	26.83
40	Shield Box B In	29.46	29.76	22.40
41	Shield Box B Out	39.31	37.15	27.41
42	Shield Box C In	39.24	37.17	26.56
43	Shield Box C Out	40.12	37.49	26.80
44	Shield Box C Out	30.88	30.88	23.44
45	Shield Box C In	31.88	31.60	22.93
46	Motor Assy.	34.07	33.69	24.56
47	Motor Assy.	33.64	33.21	25.30
48	Motor Assy.	33.62	33.02	24.29

TABLE VI

INTERNAL POWER DISSIPATION:
NORMAL POWER TESTS

	Input Power (Watts)		
	Model 1	Model 2	Model 3
Box A			
Divider A	69.21	-	3.15
Divider B	34.51	-	1.57
Total	103.72	32.69	4.72
Box B			
Divider A	13.85	4.44	0.64
Divider B	27.70	8.66	1.26
Total	41.55	13.10	1.90
Box C			
Divider A	14.00	4.40	0.64
Divider B	6.94	2.19	0.32
Total	20.94	6.59	0.96
Total Model Power	166.21	52.38	7.58

TABLE VII

DOUBLE POWER TEST RESULTS
(models insulated on top and bottom)

T.C.No.	Location	Temperatures (°C) Model 1	Model 2	Model 3
1	Box A Face	97.09	96.49	93.78
2	Box A Face	86.11	90.35	84.80
3	Box A Face	80.91	81.72	77.51
4	Box C Face	80.80	81.74	74.53
5	Box C Face	98.13	95.40	81.48
6	Box C Face	109.90	103.53	86.41
7	Box B Face	109.25	103.26	86.26
8	Box B Face	91.85	91.06	78.20
9	Box B Face	80.24	80.82	74.15
10	Frame I Bottom	88.78	86.20	77.36
11	Frame I Top	88.62	86.37	80.47
12	Frame II Top	80.53	80.40	74.07
13	Frame II Bottom	81.09	81.11	73.11
14	Frame III Top	101.43	96.91	82.27
15	Frame III Bottom	101.98	96.53	81.87
16	Frame I Top	88.31	86.52	78.98
17	Frame I Bottom	88.16	86.20	76.49
18	Frame II Bottom	82.18	81.85	73.93

TABLE VII (Continued)

T.C.No.	Location	Temperatures (°C) Model 1	Model 2	Model 3
19	Frame II Top	81.48	80.89	74.33
20	Frame III Top	100.98	96.32	82.25
21	Frame III Bottom	101.49	96.46	81.15
22	Box C Top	86.61	85.24	77.07
23	Box C Bottom	86.41	84.60	75.40
24	Box C Bottom	102.19	96.40	81.10
25	Box C Top	101.91	97.46	82.13
26	Box B Top	100.43	95.74	81.87
27	Box B Bottom	101.23	96.28	80.80
28	Box B Top	80.44	80.51	74.27
29	Box B Bottom	81.83	81.22	73.42
30	Box A Top	78.82	77.93	73.27
31	Box A Bottom	79.24	78.07	71.73
32	Box A Top	87.83	85.57	80.51
33	Box A Bottom	88.00	84.24	77.00
34	Shield Box A Out	101.02	98.65	93.48
35	Shield Box A In	99.30	99.06	93.22
36	Shield Box A In	89.43	89.48	83.20
37	Shield Box A Out	87.39	86.70	81.30
38	Shield Box B Out	85.39	84.91	76.58

TABLE VII (Continued)

T.C.No.	Location	Temperatures (°C) Model 1	Model 2	Model 3
39	Shield Box B In	102.13	98.89	84.96
40	Shield Box B In	88.40	87.50	77.82
41	Shield Box B Out	105.57	100.00	85.94
42	Shield Box C In	103.66	99.34	84.44
43	Shield Box C Out	106.11	100.34	84.73
44	Shield Box C Out	89.65	88.31	78.91
45	Shield Box C In	92.78	90.72	79.36
46	Motor Assy.	96.11	93.46	80.76
47	Motor Assy.	94.15	92.52	82.33
48	Motor Assy.	94.98	92.54	80.87

TABLE VIII

INTERNAL POWER DISSIPATION:
DOUBLE POWER TESTS

	Input Power (Watts)		
	Model 1	Model 2	Model 3
Box A			
Divider A	136.16	--	6.63
Divider B	69.49	--	3.33
Total	205.65	64.83	9.96
Box B			
Divider A	27.88	8.91	1.28
Divider B	56.04	17.56	2.55
Total	83.92	26.47	3.83
Box C			
Divider A	28.18	8.94	1.29
Divider B	14.05	4.40	0.65
Total	42.23	13.34	1.94
Total Model Power	331.80	104.64	15.73

TABLE IX

THREE-DIMENSIONAL TEST RESULTS
(insulation removed on top of model)

T.C.No.	Location	Temperatures (°C) Model 1	Model 2	Model 3
1	Box A Face	36.62	35.76	35.45
2	Box A Face	29.61	32.37	28.93
3	Box A Face	25.95	26.78	23.78
4	Box C Face	23.54	23.24	19.42
5	Box C Face	32.56	30.44	23.20
6	Box C Face	39.14	34.90	25.95
7	Box B Face	39.29	35.55	26.68
8	Box B Face	30.41	29.24	22.30
9	Box B Face	24.54	23.78	20.12
10	Frame I Bottom	28.93	27.22	22.72
11	Frame I Top	23.49	23.37	20.82
12	Frame II Top	19.68	20.02	17.22
13	Frame II Bottom	24.83	24.17	20.18
14	Frame III Top	30.54	28.54	22.50
15	Frame III Bottom	34.68	30.90	23.24
16	Frame I Top	23.34	23.15	19.98
17	Frame I Bottom	27.76	26.41	21.59
18	Frame II Bottom	24.83	24.20	19.90

TABLE IX (Continued)

T.C.No.	Location	Temperatures (°C) Model 1	Model 2	Model 3
19	Frame II Top	21.10	20.48	18.12
20	Frame III Top	31.43	28.29	23.29
21	Frame III Bottom	34.49	31.00	23.29
22	Box C Top	22.28	22.60	19.28
23	Box C Bottom	26.71	25.32	20.28
24	Box C Bottom	34.93	30.98	23.20
25	Box C Top	31.88	29.20	22.48
26	Box B Top	30.37	28.41	24.51
27	Box B Bottom	34.80	31.45	23.32
28	Box B Top	20.22	21.20	18.65
29	Box B Bottom	25.00	24.15	20.20
30	Box A Top	17.82	18.15	16.48
31	Box A Bottom	24.51	23.71	19.95
32	Box A Top	23.88	23.49	21.27
33	Box A Bottom	29.63	27.76	23.63
34	Shield Box A Out	37.73	36.17	34.56
35	Shield Box A In	36.29	36.48	33.69
36	Shield Box A In	28.88	29.00	26.41
37	Shield Box A Out	28.34	27.80	25.85
38	Shield Box B Out	26.00	25.28	21.17
39	Shield Box B In	35.55	32.85	25.98

TABLE IX (Continued)

T.C.No.	Location	Temperatures (°C) Model 1	Model 2	Model 3
40	Shield Box B In	26.76	25.82	21.24
41	Shield Box B Out	36.95	33.12	26.59
42	Shield Box C In	35.67	32.29	24.73
43	Shield Box C Out	36.71	32.63	25.08
44	Shield Box C Out	27.44	26.37	21.37
45	Shield Box C In	28.27	26.93	21.29
46	Motor Assy.	28.90	27.10	21.29
47	Motor Assy.	28.71	27.05	22.18
48	Motor Assy.	28.46	26.83	21.29

TABLE X

INTERNAL POWER DISSIPATION:
THREE-DIMENSIONAL TESTS

	Input Power (Watts)		
	Model 1	Model 2	Model 3
Box A			
Divider A	77.35	--	3.53
Divider B	38.71	--	1.76
Total	116.06	36.64	5.29
Box B			
Divider A	15.44	4.94	0.71
Divider B	30.88	9.65	1.41
Total	46.32	14.59	2.11
Box C			
Divider A	15.63	4.90	0.71
Divider B	7.74	2.45	0.36
Total	23.37	7.35	1.07
Total Model Power	185.75	58.58	8.46

TABLE XI

COMPARISON OF TEMPERATURES:
MODEL 1 - MODEL 2

T.C. No.	Location	$T_{M1} - T_{M2}$ (°C) Normal Power	Double Power	Three-dimensional
1	Box A Face	-0.04	0.60	0.86
2	Box A Face	-2.73	-4.24	-2.76
3	Box A Face	-0.95	-0.81	-0.83
4	Box C Face	-0.98	-0.94	0.30
5	Box C Face	0.77	2.73	2.12
6	Box C Face	2.69	6.37	4.24
7	Box B Face	2.00	5.99	3.74
8	Box B Face	-0.26	0.79	1.17
9	Box B Face	-0.61	-0.58	0.76
10	Frame I Bottom	0.66	2.58	1.71
11	Frame I Top	0.39	2.25	0.12
12	Frame II Top	-0.46	0.13	-0.34
13	Frame II Bottom	-0.58	-0.02	0.66
14	Frame III Top	1.40	4.52	2.00
15	Frame III Bottom	2.29	5.45	3.78
16	Frame I Top	0.14	1.79	0.19
17	Frame I Bottom	0.30	1.96	1.35

TABLE XI (Continued)

T.C. No.	Location	$T_{M1} - T_{M2}$ (°C) Normal Power	Double Power	Three-dimensional
18	Frame II Bottom	-0.58	0.33	0.63
19	Frame II Top	-0.34	0.59	0.62
20	Frame III Top	1.30	4.66	3.14
21	Frame III Bottom	1.98	5.03	3.49
22	Box C Top	0.13	1.37	-0.32
23	Box C Bottom	0.29	1.81	1.39
24	Box C Bottom	2.53	5.79	3.95
25	Box C Top	1.46	4.45	2.68
26	Box B Top	1.20	4.69	1.96
27	Box B Bottom	1.98	4.95	3.35
28	Box B Top	-0.74	-0.07	-0.98
29	Box B Bottom	-0.26	0.61	0.85
30	Box A Top	-0.16	0.89	-0.33
31	Box A Bottom	0.05	1.17	0.80
32	Box A Top	0.44	2.26	0.39
33	Box A Bottom	1.19	3.76	1.87
34	Shield Box A Out	0.55	2.37	1.56
35	Shield Box A In	-0.29	0.24	-0.19
36	Shield Box A In	-0.81	-0.05	-0.12

TABLE XI (Continued)

T.C. No.	Location	$T_{M1} - T_{M2}$ (°C) Normal Power	Double Power	Three-dimensional
37	Shield Box A Out	-0.54	0.69	0.54
38	Shield Box B Out	-0.53	0.48	0.72
39	Shield Box B In	1.36	3.24	2.70
40	Shield Box B In	-0.30	0.90	0.94
41	Shield Box B Out	2.16	5.57	3.83
42	Shield Box C In	2.07	4.32	3.38
43	Shield Box C Out	2.63	5.77	4.08
44	Shield Box C Out	0.00	1.34	1.07
45	Shield Box C In	0.28	2.06	1.34
46	Motor Assy.	0.38	2.65	1.80
47	Motor Assy.	0.43	1.63	1.66
48	Motor Assy.	0.60	2.44	1.63

TABLE XII

COMPARISON OF TEMPERATURES:
MODEL 1 - MODEL 3

T.C. No.	Location	$T_{M1} - T_{M3}$ (°C) Normal Power	Double Power	Three-dimensional
1	Box A Face	1.99	3.31	1.17
2	Box A Face	1.59	1.31	0.68
3	Box A Face	2.91	3.40	2.17
4	Box C Face	5.15	6.27	4.12
5	Box C Face	10.63	16.65	9.36
6	Box C Face	14.33	23.49	13.19
7	Box B Face	13.38	22.99	12.61
8	Box B Face	8.99	13.65	8.11
9	Box B Face	5.42	6.09	4.42
10	Frame I Bottom	7.07	11.42	6.21
11	Frame I Top	4.92	8.15	2.67
12	Frame II Top	4.22	6.46	2.46
13	Frame II Bottom	5.47	7.98	4.65
14	Frame III Top	11.63	19.16	8.04
15	Frame III Bottom	12.80	20.11	11.44
16	Frame I Top	5.90	9.29	3.36
17	Frame I Bottom	7.18	11.67	6.15

TABLE XII (Continued)

T.C. No.	Location	$T_{M1} - T_{M3}$ (°C) Normal Power	Double Power	Three-dimensional
18	Frame II Bottom	5.89	8.25	4.93
19	Frame II Top	5.12	7.15	2.98
20	Frame III Top	11.02	18.73	8.14
21	Frame III Bottom	12.56	20.34	11.20
22	Box C Top	6.50	9.54	3.00
23	Box C Bottom	7.43	11.01	6.43
24	Box C Bottom	12.95	21.09	11.73
25	Box C Top	12.07	19.78	9.40
26	Box B Top	10.86	18.56	5.86
27	Box B Bottom	12.57	20.43	11.48
28	Box B Top	4.87	6.17	1.57
29	Box B Bottom	6.26	8.41	4.80
30	Box A Top	4.07	5.55	1.34
31	Box A Bottom	5.40	7.51	4.56
32	Box A Top	4.28	7.32	2.61
33	Box A Bottom	6.93	11.00	6.00
34	Shield Box A Out	4.47	7.54	3.17
35	Shield Box A In	3.99	6.08	2.60
36	Shield Box A In	3.75	6.23	2.47

TABLE XII (Continued)

T.C. No.	Location	$T_{M1} - T_{M3}$ (°C) Normal Power	Double Power	Three-dimensional
37	Shield Box A Out	3.63	6.09	2.49
38	Shield Box B Out	6.31	8.81	4.83
39	Shield Box B In	11.34	17.18	9.57
40	Shield Box B In	7.06	10.58	5.52
41	Shield Box B Out	11.90	19.63	10.36
42	Shield Box C In	12.68	19.22	10.94
43	Shield Box C Out	13.32	21.38	11.63
44	Shield Box C Out	7.44	10.74	6.07
45	Shield Box C In	8.91	13.42	6.98
46	Motor Assy.	9.51	15.35	7.61
47	Motor Assy.	8.34	11.82	6.53
48	Motor Assy.	9.33	14.11	6.17

V. DISCUSSION

A. TEST RESULTS

In this section, we will discuss the measured temperatures of most significance to the thermal modeling problem. In most cases we will reference the measured temperatures of Models 2 and 3 to those measured for Model 1--which, in our case, could be considered the prototype.

A typical temperature distribution pattern illustrating the magnitude of the circumferential gradients for Model 1 is shown in Figure 7. The data are for a normal power test. The maximum gradient within a box is of the order of 15°C, as measured at the mid-plane. We have indicated on this figure the low and high emittance areas and the input powers (watts) for this test. This pattern is typical for all tests; however, the temperature level and the magnitude of the gradients increase at double power.

In the previous section we have tabulated the temperature differences between Models 1 and 2 and 1 and 3 at identical geometric locations (Tables XI and XII). From Table XI, it can be seen that the largest single temperature difference between Models 1 and 2 is 2.73°C (0.9%), 6.37°C (1.7%), and 4.08°C (1.4%), respectively, for the normal power, double power, and three-dimensional tests. (The percentages refer to the absolute temperature level.) The same comparison applied to Models 1 and 3 indicates that the differences are 12.57°C (4.1%), 23.49°C (6.2%), and 13.19°C (4.2%) for the three test conditions in the above order. These figures represent the worst case, and the average differences are considerably below these figures.

A comparison of the average box temperature (at mid-plane) for each of the three models at each test condition is presented in Table XIII. The average mid-plane temperature is used in these comparisons simply because the mean temperature cannot be defined adequately by three data points when there are two line sources of heat and a difference in the radiative characteristics along the box. The agreement between Models 1 and 2 is remarkably good for the three tests. The maximum difference is less than one percent of the absolute temperature, and this occurs at the double power condition. The average box temperatures of Model 3 are lower than those measured for Model 1 by approximately three percent for normal power and four percent for the double power tests. This temperature difference of four percent represents a considerable difference (16 percent) in the power dissipation. We believe that the insulation heat leaks in Model 3 represent a significant fraction of this error. This effect can be noted by comparing the percentage differences for the normal power (both ends insulated) and the three-dimensional tests where one end was uninsulated. The percentage difference is decreased when one end is uninsulated.

Theoretically, the mean temperature should increase by 19 percent for a two-fold increase in power. In computing the average temperatures, we find that the increase is approximately this amount for all tests. Apparently, the average temperature of these readings is close to the mean temperature for each of the boxes.

TABLE XIII

AVERAGE BOX TEMPERATURES
(°C)

		Model 1	Model 2	Model 3
Box A	Normal Power	31.1	32.3	28.9
	Double Power	88.0	89.5	85.5
	Three-dimensional	30.7	31.6	29.4
Box B	Normal Power	32.7	32.4	23.5
	Double Power	93.5	91.5	79.5
	Three-dimensional	31.4	29.5	23.0
Box C	Normal Power	34.4	33.5	24.4
	Double Power	96.4	93.5	80.6
	Three-dimensional	31.8	29.5	22.9

In Table XIV, we have tabulated the temperature differences measured by two thermocouples at the mid-plane of the boxes. The thermocouple locations are referenced to Figure 5. These temperature differences are representative of the gradients in the boxes. The gradients occur because of the nonuniform internal power dissipation in the two dividers. From Table XIV, it can be seen that the gradients measured for Box A are roughly equivalent for all three models. However, the gradients in Boxes B and C differ between models. For Model 3 the gradients are less than half those measured for Model 1. The source of this error was pointed out by members of the JPL technical staff, and is extremely important with respect to the feasibility of scaling spacecraft on a small scale. In the design of the three thermal models we computed the wall thicknesses of the boxes for each model from the scaling ratios using conductivity values for Armco iron, SAE 4130 and 304 stainless steel. Boxes B anc C were gold plated to approximately the same thickness (on both sides) on each model. Since the boxes on Model 3 were made of a low conductivity material and were thin, the conductance of the high conductivity plating was of the same order of magnitude as the box wall. We overlooked this rather obvious point, and therefore the conductances of Boxes B and C of Model 3, in particular, were much greater than they should have been. Box A was not plated and therefore we would expect the gradients to be equivalent from model to model.

For scaled lengths, the temperature gradients in the walls of the boxes are related by

$$\frac{\Delta T_1}{\Delta T_2} = \frac{q_1}{q_2} \frac{C'_2}{C'_1}$$

where: q = heat flow (assumed to be scaled)

C' = conductance of wall

For a plating thickness, δ, applied to both sides of the box wall, the conductance is

$$C' = 2\delta\bar{k}_p + k\,t$$

where $\bar{k}_p$ = mean conductivity of plating

k = wall conductivity

t = wall thickness

Using the plating thicknesses presented in C-3, and a mean conductivity of 4 watts/cm°K for the plating, we have computed the approximate ratios of the gradients for scaled input power ratios. (The subscripts refer to the model.)

	Box B	Box C
$\frac{\Delta T_1}{\Delta T_2}$ (calculated)	1.10	1.19
$\frac{\Delta T_1}{\Delta T_2}$ (measured)	1.22	1.31
$\frac{\Delta T_1}{\Delta T_3}$ (calculated)	1.95	2.82
$\frac{\Delta T_1}{\Delta T_3}$ (measured)	2.19	2.45

From the above tabulation, one can see that the errors in the temperature gradients introduced by the non-scaled elements (i.e., the thermal control coatings) are significant. It can be seen also that we can explain the differences by accounting for the added conductance of the coating. Note that the plating was also applied to the simulated joint conductance tabs. Therefore, these were essentially non-scaled elements in Model 3 where the effects of the coating are most significant.

TABLE XIV

BOX TEMPERATURE GRADIENTS
(°C)

		Model 1	Model 2	Model 3
Box A	$(T_1 - T_3)$			
	Normal Power	9.76	8.86	10.69
	Double Power	16.18	14.77	16.27
Box B	$(T_7 - T_9)$			
	Normal Power	14.48	11.87	6.62
	Double Power	29.01	22.44	12.11
Box C	$(T_6 - T_4)$			
	Normal Power	15.50	11.83	6.32
	Double Power	29.1	21.79	11.98

In Table XV we have summarized the temperature gradients between the boxes and the frames in the vicinity of the simulated joint conductances. In most of the tabs, the temperature gradients were too small to measure with our thermocouples which were arranged to measure absolute rather than differential temperatures. In Table XV we have only listed the gradients for two locations at the double power condition where the magnitudes of the measurements were larger than the uncertainty interval in the measurements. The purpose of this table is to show the magnitude of the gradients rather than to compare values between models. In effect, the conductive coupling between boxes and frames through the simulated joint conductances was large. With a large conductance, it would be difficult to assess the differences between models caused by an increase in joint conductance. The increase in joint conductance was due to the non-scaled plating on the tabs. It should be noted that one additional test was completed with Model 1 to determine whether the boxes were well-coupled conductively. In this test, the boxes were radiatively shielded from the mid-course guidance motor and from each other by a low emittance shield. The results indicated that the temperatures were identical (within thermocouple accuracy) to those measured without the shields at the same power level. Therefore, we conclude that the heat flowing between adjacent boxes was conducted through the tabs used to simulate a joint conductance.

TABLE XV

SIMULATED JOINT CONDUCTANCE TEMPERATURE GRADIENTS:
DOUBLE POWER TESTS
(°C)

		Model 1	Model 2	Model 3
Box A	(Frame I)			
	$T_{12} - T_{30}$ (top)	1.71	2.47	0.80
	$T_{13} - T_{31}$ (bottom)	1.85	3.04	1.38
Box C	(Frame II)			
	$T_{16} - T_{22}$ (top)	1.70	1.28	1.91
	$T_{17} - T_{23}$ (bottom)	1.75	1.60	1.09

Note: Other temperature gradients were less than thermocouple accuracy.

The axial temperature gradients in each of the boxes for the three-dimensional tests are presented in Table XVI. The differences were measured on the top and bottom of each box in the vicinity of the joint conductance tabs. In this case, the increased wall conductance (non-scaled plating effects) for Models 2 and 3 decreases the gradients. The effect is most pronounced in Box C, as expected. Apparently, the gradients in Box A are decreased by the increased wall conductance of the two adjacent boxes.

B. UNCERTAINTY ANALYSIS

In this section, we will attempt to estimate the effects of uncertainties in properties, instrumentation heat leaks, etc., on the mean temperature of the models by considering the models as essentially isothermal. Although it would be fortuitous if we could compute a single uncertainty interval for all measured temperatures, the relative importance of uncertainties in the variables can be identified by analysis.

The uncertainties involved in reproducing identical spatial temperature distributions in thermal modeling experiments arise from three major sources. The first source of uncertainties is inherent to the models themselves, i.e., those uncertainties arising from deviations in a perfect scale of geometry, thermal radiation characteristics, thermal conductivities, and internal heat sources. A second uncertainty is involved with the relationship between model size and the size of the test chamber. The heat leaks through paths provided by thermocouple wires, heater power leads, insulation, and the gaps between boxes which are not scaled exactly, constitute a third source of uncertainty.

TABLE XVI

AXIAL TEMPERATURE GRADIENTS: THREE-DIMENSIONAL TESTS
(°C)

		Model 1	Model 2	Model 3
Box A				
	Frame I	6.69	5.56	3.47
	Frame II	5.75	4.27	2.36
Box B				
	Frame I	4.78	2.95	1.55
	Frame III	4.43	3.04	1.19
Box C				
	Frame II	4.43	2.72	1.00
	Frame III	3.05	1.78	0.72

An analysis of the uncertainties arising from the first source must, of necessity, be approximate. It is theoretically possible to use measured temperature data from a single model and obtain the temperature differences which would result in a model having scaled deviations in lengths, powers, etc. For instance, one can predict the changes in the temperatures (the uncertainty interval) at all measured points in a thermal scale model which would result from an uncertainty interval in the scaled length, only if all lengths are changed by the same fraction. The changes in the temperature distribution due to deviations in the geometry which do not preserve geometric similitude are not predictable by dimensional analysis of test data. Similarly, one can predict the temperature difference which would arise due to imperfect scaling of internal power sources if all sources deviated by the same percentage, but one cannot predict temperature deviations resulting from random differences in the scaled input from several power sources. It is necessary to have a complete mathematical model of the test system in order to complete an uncertainty analysis which accounts for deviations in thermal scale.

Irrespective of the limitations of an uncertainty analysis which does not require complex machine computations, it is instructive to pursue such an analysis in order to estimate the temperature differences that might be expected from uncertainties inherent to model construction. Within the constraints of our thermal modeling tests, dimensional analysis predicts that the temperature data at a given location on the model and all scaled versions of it can be correlated

on the basis of two dimensionless parameters, ϕ and ψ. Their functional relationship can be shown on a plot such as Figure 8. Similar curves can be obtained for each point on the model(s) where temperature is measured, and ϕ as a function of ψ for each point can be obtained by testing with varying values of input power q, for instance. Now, referring to Figure 8,

$$\Delta\phi = \alpha\Delta\psi \tag{1}$$

$$\phi = \beta\psi \tag{2}$$

$$\frac{\Delta\phi}{\phi} = \frac{\alpha}{\beta}\,\frac{\Delta\psi}{\psi} \tag{3}$$

$$\frac{\Delta\phi}{\phi} = \frac{\Delta q}{q} - \frac{\Delta L}{L} - \frac{\Delta K}{K} - \frac{\Delta T}{T} \tag{4}$$

and

$$\frac{\Delta\psi}{\psi} = \frac{\Delta\bar{\epsilon}}{\bar{\epsilon}} + 3\,\frac{\Delta q}{q} - 2\,\frac{\Delta L}{L} - 4\,\frac{\Delta K}{K} \tag{5}$$

Therefore

$$\frac{\Delta T}{T} = \left(1 - 3\,\frac{\alpha}{\beta}\right)\frac{\Delta q}{q} + \left(2\,\frac{\alpha}{\beta} - 1\right)\frac{\Delta L}{L} + \left(4\,\frac{\alpha}{\beta} - 1\right)\frac{\Delta K}{K} - \left(\frac{\alpha}{\beta}\right)\frac{\Delta\bar{\epsilon}}{\bar{\epsilon}} \tag{6}$$

Equation 6 provides the basis for computing the percentage change in temperature at each location resulting from percentage changes in the characteristics of the model(s). The symbol $\bar{\epsilon}$ is used here to denote an area-averaged emittance; however, inherent in the analysis is the assumption that the emittances at all surfaces deviate by the same percentage. Similarly, all the internal powers, q, at geometrically similar points must vary by the same percentage; all lengths, L, must vary by the same percentage, etc.

If $\alpha = 0$ and ϕ = constant, the temperature distributions are controlled by solid conduction. If $\frac{\alpha}{\beta} = \frac{1}{4}$ at all locations, it can be shown that the model approximates an isothermal system whose temperature is controlled by radiation from its exterior surfaces to an infinite thermal sink. The test data obtained in our experiments at two power levels is not sufficient to allow us to determine the value of α at any of the temperature measuring points on the models. Therefore, we cannot determine α/β and use Equation 6 to predict uncertainties. However, our models do approximate a system in which $\alpha/\beta = 1/4$ at all points, and we assume this value in lieu of more complete data. With this assumption, Equation 6 reduces to

$$\frac{\Delta T}{T} = \frac{1}{4}\frac{\Delta q}{q} - \frac{1}{2}\frac{\Delta L}{L} - \frac{1}{4}\frac{\Delta \bar{\epsilon}}{\bar{\epsilon}} \qquad (7)$$

Interestingly enough, we note no effect of thermal conductivity changes on the temperatures. This is the direct result of our assumption of $\alpha/\beta = 1/4$ at all points, which presupposes the use of materials having thermal conductivities high enough to make the systems essentially isothermal. This assumption eliminates from consideration the effect of finite thermal conductivities which produce temperature gradients in the models.

The maximum percentage uncertainty in temperature, T, for a given model resulting from scale changes in q, L, and $\bar{\epsilon}$ expressed in percent can be computed by substituting, in Equation 7, estimates of the uncertainties in each of these values which are appropriate to the experiments. For instance, if the estimate of the uncertainties $\frac{\Delta q}{q}$, $\frac{\Delta L}{L}$, and $\frac{\Delta \bar{\epsilon}}{\bar{\epsilon}}$ are all one percent, then the maximum uncertainty in T is

$$\left.\frac{\Delta T}{T}\right|_{max} = \frac{1}{4}(1) + \frac{1}{2}(1) + \frac{1}{4}(1) = 1\% \qquad (8)$$

Because of the number of variables involved, it is preferable to consider the most probable uncertainty in temperature based on equal odds that the uncertainty interval in each of the variables propagates the final uncertainty. In this case, the most probable uncertainty in temperature is

$$\frac{\Delta T}{T} = \sqrt{\left(\frac{1}{4}\frac{\Delta q}{q}\right)^2 + \left(\frac{1}{2}\frac{\Delta L}{L}\right)^2 + \left(\frac{1}{4}\frac{\Delta \bar{\epsilon}}{\bar{\epsilon}}\right)^2} \qquad (9)$$

The most probable difference in temperature between two models designed for identical temperature distributions arising from in-scale uncertainties in q, L, and $\bar{\epsilon}$ for each model is

$$\left.\frac{\Delta T}{T}\right|_{1-2} = \frac{1}{2}\left(\frac{\Delta T_1}{T_1} + \frac{\Delta T_2}{T_2}\right)$$

$$= \frac{1}{2}\sqrt{\left(\frac{1}{4}\cdot\frac{\Delta q_1}{q_1}\right)^2 + \left(\frac{1}{2}\cdot\frac{\Delta L_1}{L_1}\right)^2 + \left(\frac{1}{4}\cdot\frac{\Delta \bar{\epsilon}_1}{\bar{\epsilon}_1}\right)^2}$$

$$+ \frac{1}{2}\sqrt{\left(\frac{1}{4}\cdot\frac{\Delta q_2}{q_2}\right)^2 + \left(\frac{1}{2}\cdot\frac{\Delta L_2}{L_2}\right)^2 + \left(\frac{1}{4}\cdot\frac{\Delta \bar{\epsilon}_2}{\bar{\epsilon}_2}\right)^2} \qquad (10)$$

For Model 1, we estimate

$$\frac{\Delta q_1}{q_1} = 0.0014$$

$$\frac{\Delta L_1}{L_1} = 0.0016$$

$$\frac{\Delta \bar{\epsilon}_1}{\bar{\epsilon}_1} = 0.0175$$

For Model 3 we estimate

$$\frac{\Delta q_3}{q_3} = 0.0014$$

$$\frac{\Delta L_3}{L_3} = 0.0076$$

$$\frac{\Delta \bar{\epsilon}_3}{\bar{\epsilon}_3} = 0.0175$$

Substituting these values in Equation 10, we get

$$\left.\frac{\Delta T}{T}\right|_{1-3} = 0.0051$$

or 1/2 percent of the absolute temperature.

It is to be emphasized that the result expressed immediately above was derived on the basis of very restrictive assumptions. Most important among

these was the assumption that uncertainties in the properties of the models occurred in scale. Another important consideration bearing on the interpretation of this result was the assumption of isothermal models.

Another uncertainty involves the relationship between model size and chamber size. In our experiments, the largest and smallest models were tested in a cold wall vacuum chamber of fixed dimensions. The LN_2 shroud was coated with an optical black paint to obtain a high emittance. However, in practice, one cannot obtain an emittance of unity. Because the model dimensions were significant with respect to the shroud dimensions, the temperatures of the largest model will differ from those of the smallest model due to reflections from the "non-black" shroud. In the following paragraphs, we will estimate the magnitude of these differences using a simplified mathematical model.

Consider a spherical test model (maintained at a constant temperature T by internal power dissipation) radiating to a heat sink also maintained at a constant temperature. For diffusely reflecting "grey" surfaces, it can be shown that the following relationship holds

$$\sigma T^4 = q/A \left[\frac{1}{\epsilon_m} + \frac{A}{A_c}\left(\frac{1}{\epsilon_c} - 1\right)\right] + \sigma T_w^4$$

If we differentiate this expression, we obtain

$$\frac{\partial T}{\partial (A/A_c)} = \frac{q\left(\frac{1}{\epsilon_c} - 1\right)}{4 A \sigma T^3}$$

where: T = model temperature

T_w = chamber wall temperature

A = model area

A_c = area of heat sink

q = model internal power dissipation

ϵ_c = chamber wall emittance

ϵ_m = model emittance

If we let the subscripts 1 and 3 refer to the largest and smallest models, we note that in our normal power experiments $(q/A)_1 \cong (q/A)_3 \cong 0.0228$ watts/cm^2 and $T_1 \cong T_3 \cong 300°K$.

We assume, also, that $A_1 \cong A_c$ and from the model geometry we know that $A_1 = 22\ A_3$. From the above equation, we can compute the magnitude of the temperature difference between Models 1 and 3 for various chamber wall emittances.

ϵ_c	$T_1 - T_3$ (°C) (Normal Power)	$T_1 - T_3$ (°C) (Double Power)
1.0	0	0
0.98	0.73	0.89
0.96	1.48	1.81

Measurements of the surface emittance of the paint coatings on the LN_2 shrouds of the test chamber used in these experiments indicate that the emittance is approximately 0.97. On the basis of this conservative mathematical model, we conclude that the errors in temperature between the largest

and smallest model are less than 2°C. When the models were suspended in the chamber, we positioned the supports so that the view factor between Box A (which dissipates the largest amount of power) and the LN_2 shroud was the same for all models. In this manner, we considerably reduced these effects of model size. It should be noted here that we have not accounted for the errors due to the simulation of outer space with partially reflecting walls and a finite wall temperature. These effects are significant to thermal testing but can be analyzed separately.

The third source of temperature uncertainties is brought about by stray heat leaks in thermocouples, heater leads, insulation, etc. For this particular set of thermal models, we have made an estimate of the magnitude of these heat leaks (c.f., Section II-C). Estimates of the thermocouple heat leaks are presented in Table IV. From these estimates, we find the following percentage errors in mean temperature:

$$\frac{\Delta T_1}{T_1} = -1.0\%$$

$$\frac{\Delta T_2}{T_2} = -1.43\%$$

$$\frac{\Delta T_3}{T_3} = -1.1\%$$

These values indicate that the difference in temperature between models will be be of the order of 1.2°C due to improper thermocouple scaling. In this case,

the maximum difference in between Models 1 and 2. The differences between Models 1 and 3 is estimated to be less than 0.3°C.

The heat leaks associated with the heater leads are estimated to be 0.3% of the model power dissipation in the worst case (c.f., Section II-C6). The temperature errors are thus less than -0.1% and can be neglected.

The heat leaks associated with the "super insulation" packages are essentially unpredictable by simplified analysis because of the complex heat flow patterns which exist in regions where thermal shorts are unavoidable. We have calculated the heat flow through the insulation on Model 1 based on a one-dimensional analysis. This estimate indicated that the heat leak would be of the order of 1.3%--a temperature error of -0.3%. Our experience with such insulation systems indicates that the actual heat leak might be several times this value, due to thermal shorts. The percentage would also increase as the model size decreases, because of the increasing importance of the thermal shorts. Based on the above reasoning, we estimate that a considerable fraction of the temperature differences between Models 1 and 3 can be attributed to insulation heat losses.

Another source of errors is the improper scaling of the clearance gaps between the boxes. One might argue that these errors could be treated as deviations in a perfectly scaled geometry; however, we prefer to treat these errors as stray heat leaks, since we can estimate their influence on the model temperature. In Table I we have presented a summary of the measured gap

areas. From these measured values, we have computed the temperature differences between models attributable to the improper gap scaling. Our computations were based on the assumption that these gaps radiate as "black cavities." The results indicate that the temperature differences between Models 1 and 2 are negligible. The temperature difference between Model 1 and 3 attributable to gap errors is approximately 1/2°C.

In summary, we have computed the probable uncertainty in temperatures between models designed to have identical temperatures due to uncertainties in variables which occur in scale. The computed uncertainty interval between Models 1 and 3 was approximately 1.5°C. The errors due to testing three models of different size in a chamber of fixed dimensions was computed to be less than 2°C. The temperature errors due to inexact scaling of instrumentation leads was estimated to be 1.2°C for Model 2 and 0.3°C for Model 3. The error associated with inaccuracies in the gaps between boxes was approximately 1/2°C between Models 1 and 3. The greatest source of uncertainty in the models was the heat leak through the insulation.

Finally, one must account for the uncertainties involved in the temperature measurements. In the experimental apparatus used in this investigation, the uncertainty interval was approximately 1/2°C.

C. PROBLEM AREAS

In this section, we point out some of the practical problems which were encountered in the test program and some which we foresee in future thermal modeling work.

For the particular prototype configuration selected for the experimental study described previously, three main problem areas were encountered: (1) the control of dimensional tolerances in the scale models, (2) the instrumentation associated with supplying the internal power and measuring temperatures, and (3) the fabrication of an insulation scheme which would provide scaled heat leaks from model to model. In addition, we now recognize that the problem of the conductance of the thermal control surfaces is a limiting factor in the design of very small-scale models.

Dimensional tolerances are particularly important in small models where the wall thicknesses are below 1/32 inch. In Model 3, we encountered some difficulties in fabricating and welding the boxes to the proper dimensions with these thin wall sections. For this reason, we were forced to form the boxes in a precision jig. The welding of these thin-walled components leads to dimensional changes which are unavoidable. Furthermore, the costs associated with model fabrication are strongly influenced by the desired dimensional tolerances--particularly in sheet-metal work.

The instrumentation associated with the models was another problem area; however, in our case we scaled the thermocouple leads and more or less avoided that problem. In the realistic case where a prototype spacecraft has no external leads, the control of these heat leaks becomes more significant. In such cases, it may be necessary to resort to infrared techniques for temperature measurement in models where the internal power dissipation is small. The design of heater leads to minimize heat leaks is not difficult, and if necessary one could consider self-contained battery sources, etc.

Our experience with the model configurations tested in this study indicates that the problems associated with heat leaks from "super insulations" produced the largest uncertainties. The insulation packages for Model 3 were difficult to fabricate, and we were not satisfied with the end result. After testing Model 3 and observing that the mean temperatures were considerably lower than those of Models 1 and 2, we examined the insulation in some detail and concluded that the foils were compressed, thereby increasing the effective conductivity of the insulation. Due to limitations on the scope of the work, we were unable to rebuild the insulation and re-test Model 3.

In the previous discussion of the test results, we pointed out the source of the errors in the measured temperature gradients of Models 2 and 3. The errors were due to the introduction of non-scaled conductivities resulting from the added conductance of the plating. In certain cases, it may be possible to use a smaller wall thickness in the models to compensate for the added conductance of the plating when it is desired to scale for equivalent temperatures in model and prototype. However, it can be shown that this procedure will not be adequate when the wall thicknesses of the prototype are small. For example, in Box C of Model 3, it would have been impossible to model the temperature gradients, since the conductance of the plating alone was higher than the desired wall conductance. Thin films deposited in vacuum may be a solution to this problem, although handling of these surfaces will change their characteristics.

The joint conductance simulation techniques used in this program did not appear to be a problem area, that is, if one compares temperature distributions from model to model. However, it should be re-emphasized that we did not simulate a prototype with joints. The models in this case were scaled from a prototype having a simulated joint conductance. Where it is desired to model an actual joint in a prototype, one must first know the conductance (from measurements or calculation) and then design a simulation scheme to provide the necessary scaled conductance. Detailed analyses of the simulated joints may be required in such cases.

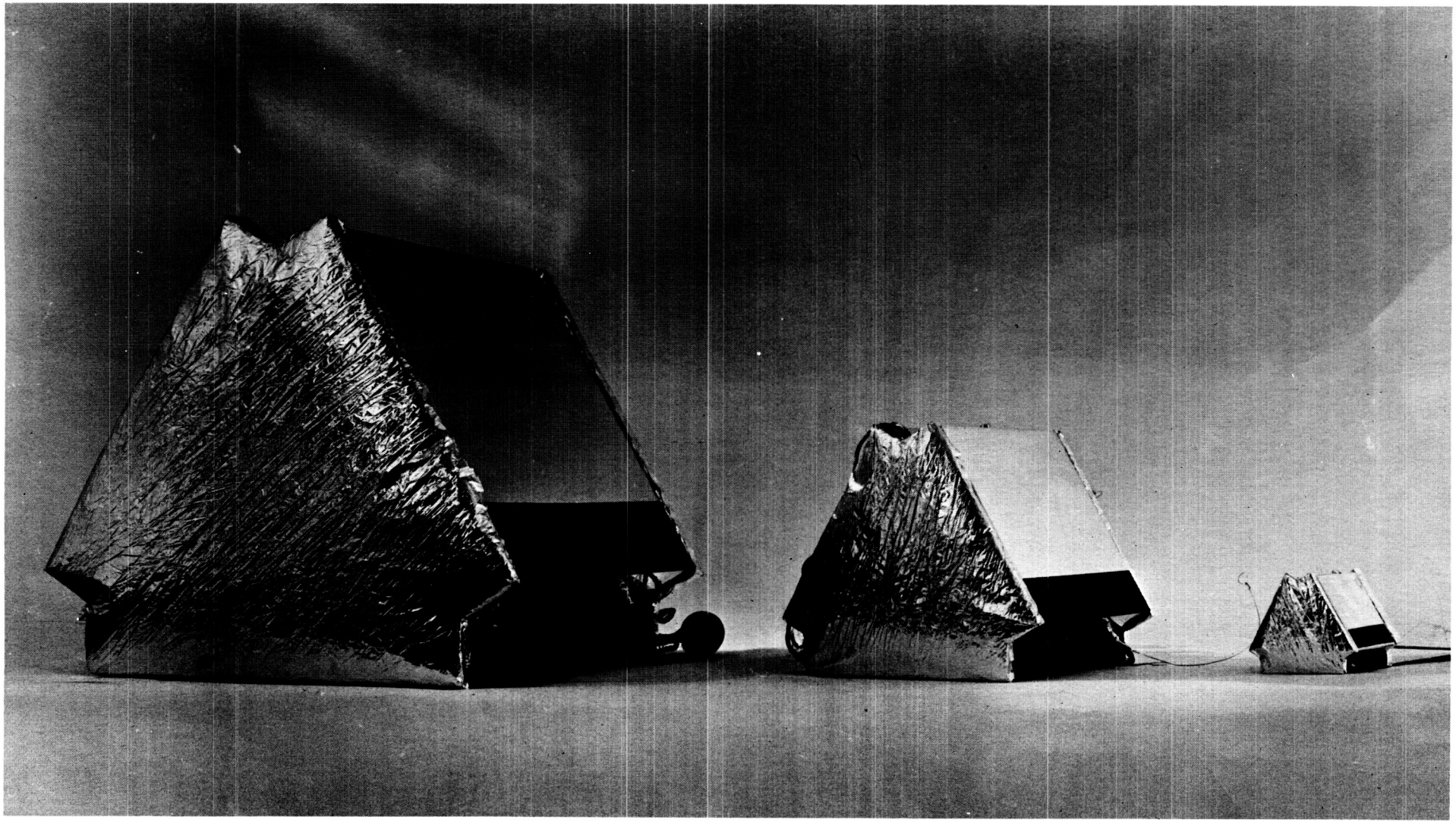

Model 1 Model 2 Model 3

FIGURE 1 PHOTOGRAPH OF THERMAL MODELS

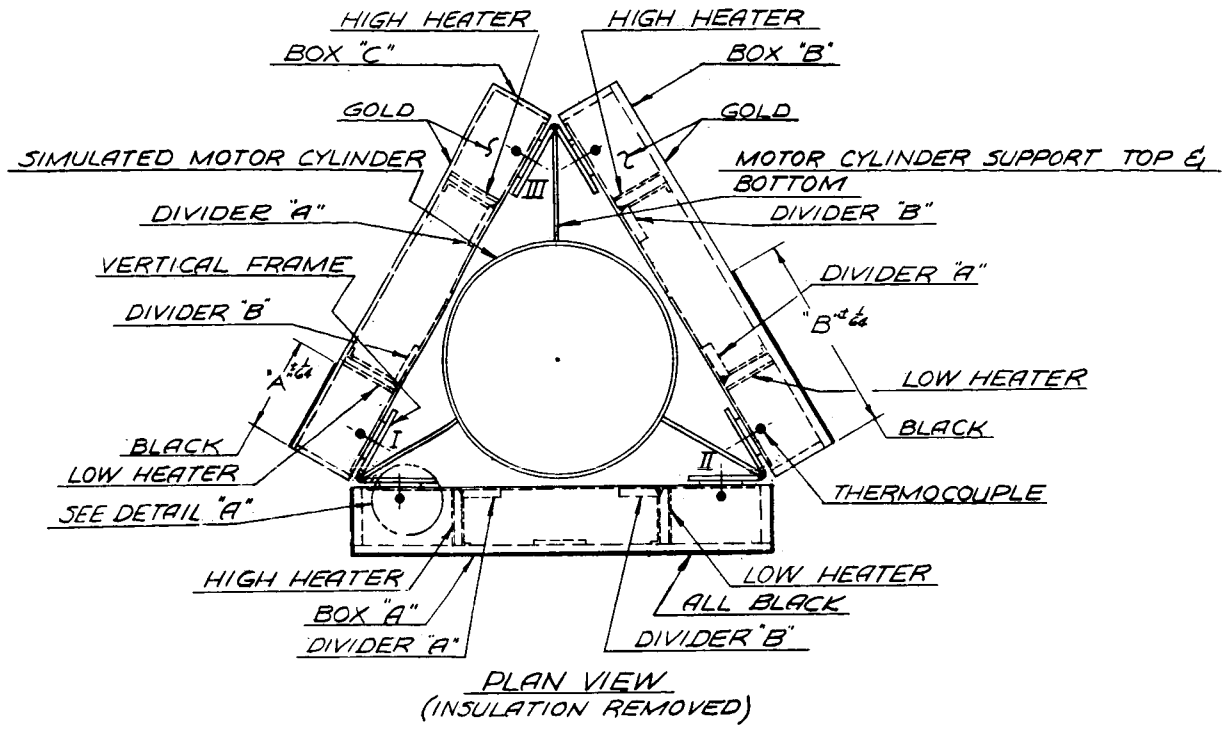

PLAN VIEW
(INSULATION REMOVED)

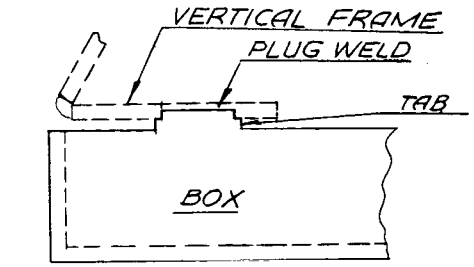

ENLARGED VIEW
DETAIL "A"

MODEL	"A"	"B"
No. 1	3 3/8	7 41/64
No. 2	1 29/32	4 19/64
No. 3	49/64	1 47/64

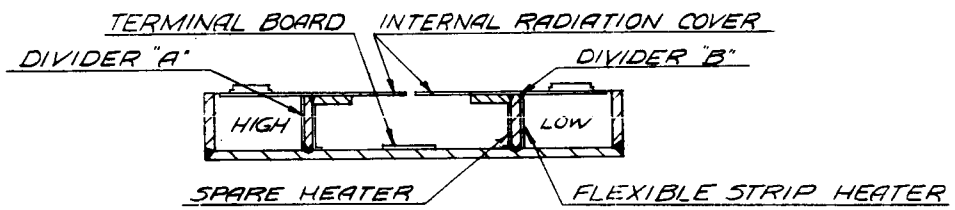

SECT. X-X

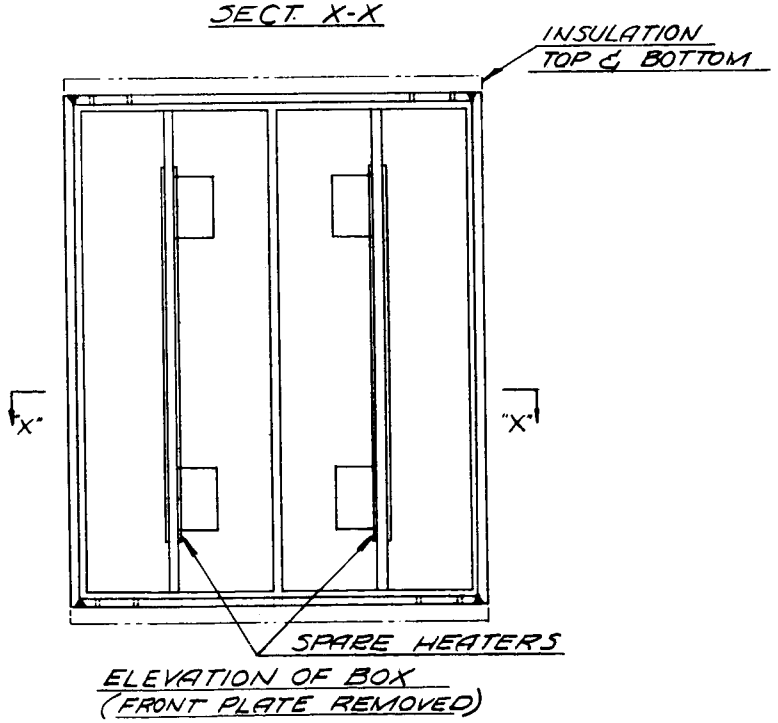

ELEVATION OF BOX
(FRONT PLATE REMOVED)

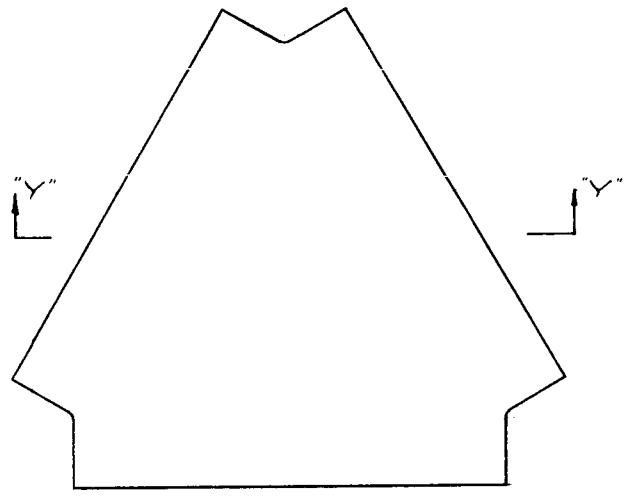

PLAN VIEW OF INSULATION

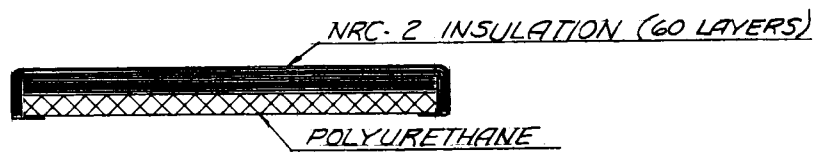

SECT. "Y-Y"

FIGURE 2 THERMAL MODEL ASSEMBLY

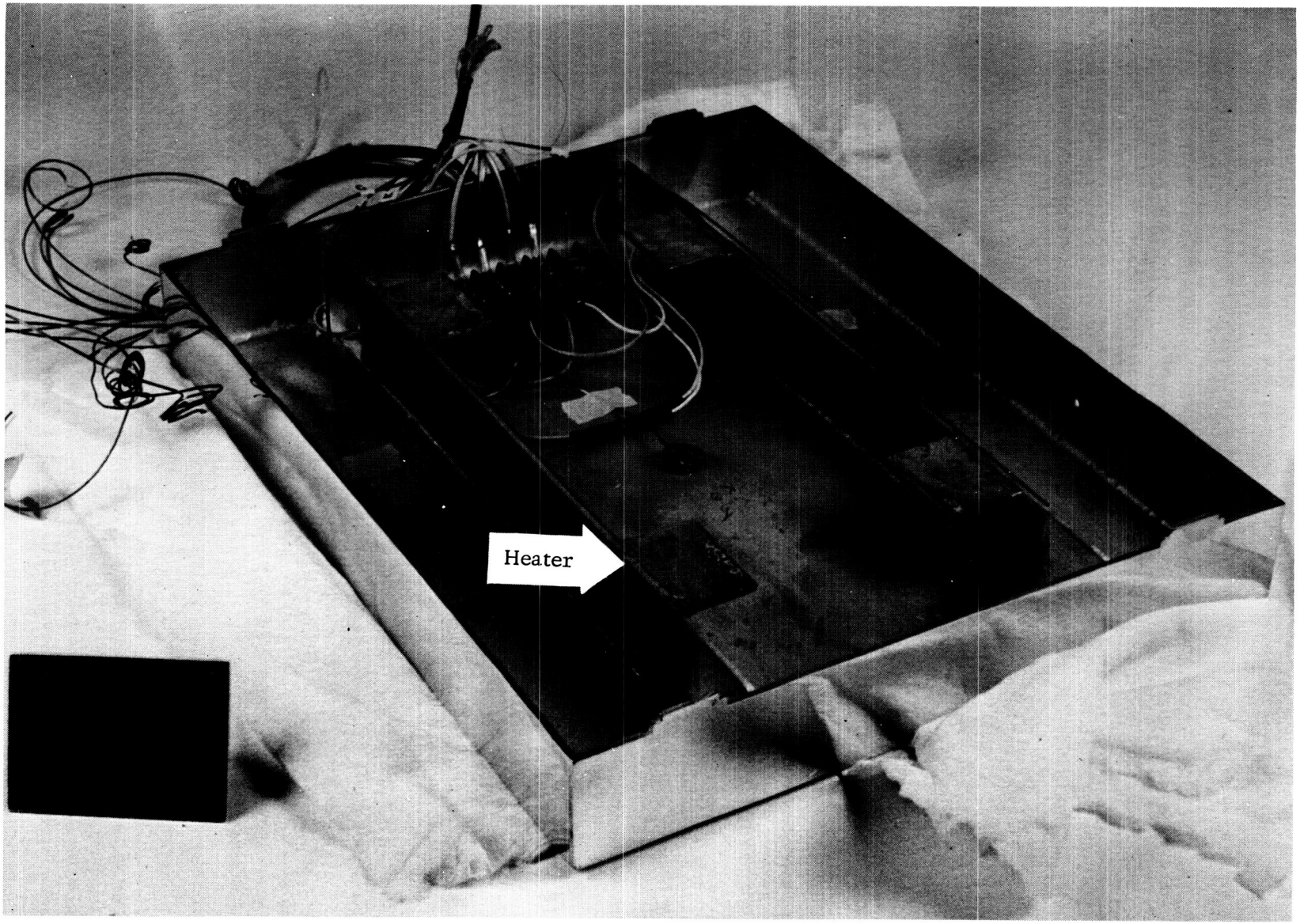

FIGURE 3 TYPICAL HEATER INSTALLATION

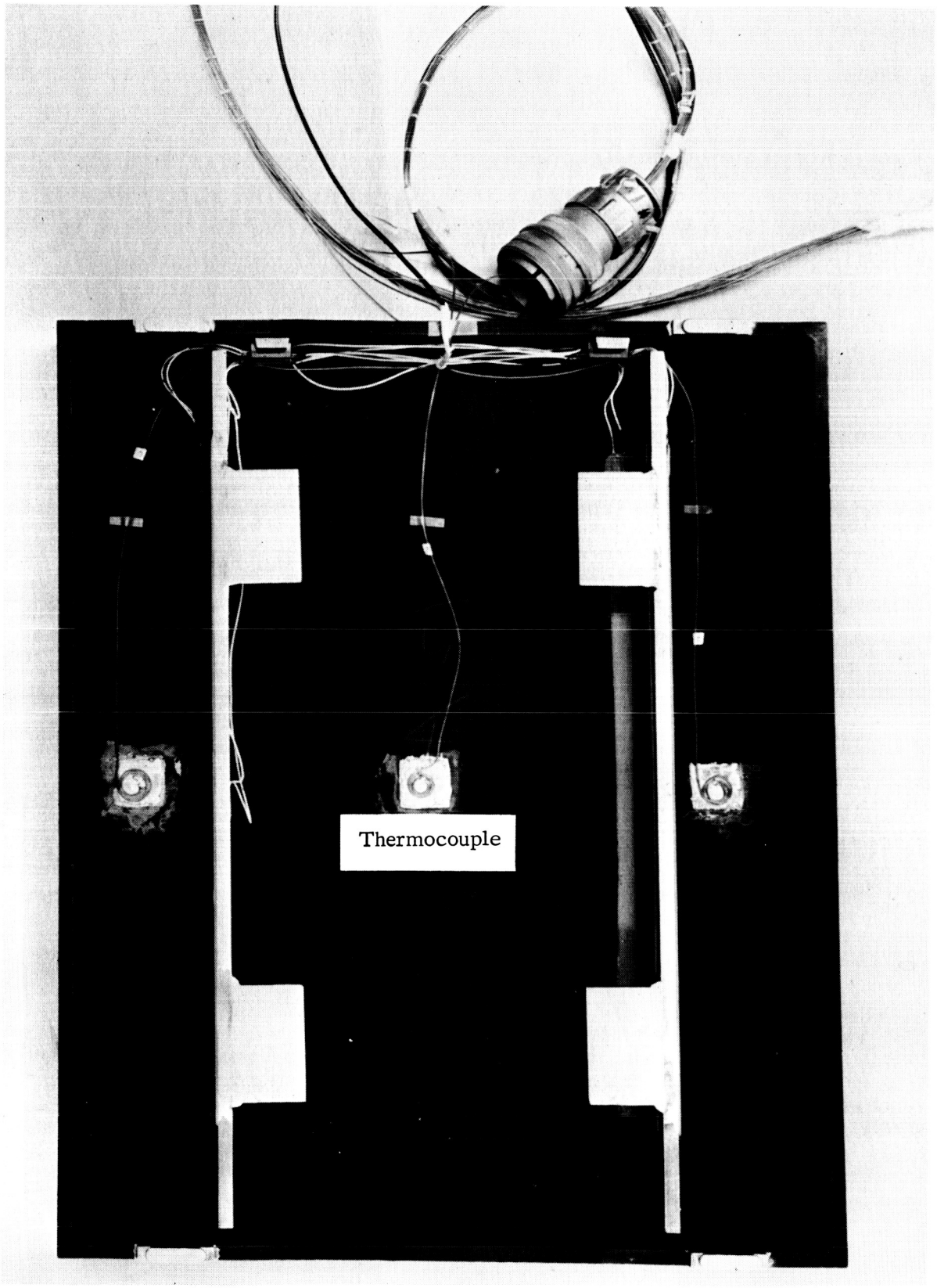

FIGURE 4 TYPICAL THERMOCOUPLE INSTALLATION

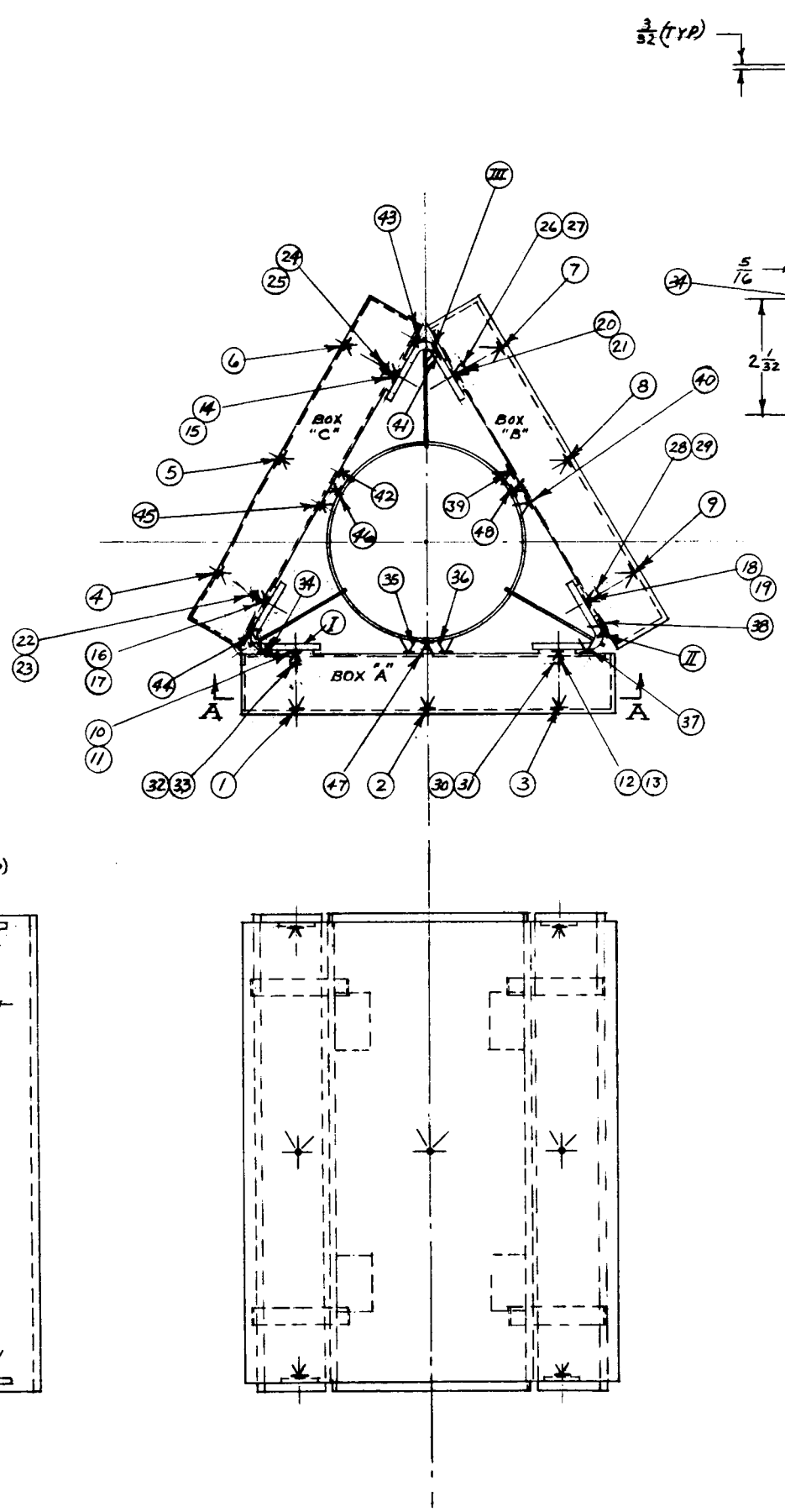

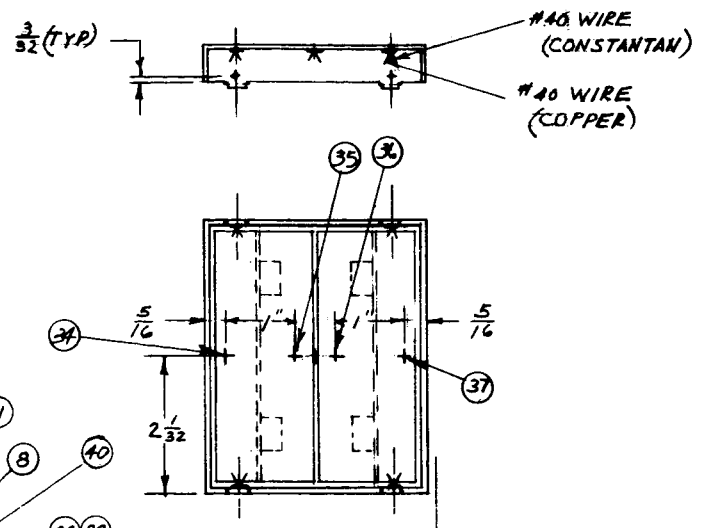

TYPICAL SECTION A-A SHOWING THERMOCOUPLE LOCATIONS ON RADIATION SHIELDS

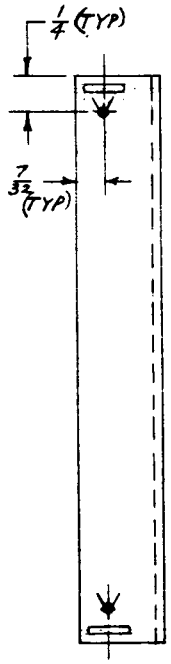

48	1	MOTOR ASS'Y	THERMOCOUPLE
47	1	MOTOR ASS'Y	
46	1	MOTOR ASS'Y	
45	1	SHIELD BOX "C" (IN)	
44	1	SHIELD BOX "C" (OUT)	
43	1	SHIELD BOX "C" (OUT)	
42	1	SHIELD BOX "C" (IN)	
41	1	SHIELD BOX "B" (OUT)	
40	1	SHIELD BOX "B" (IN)	
39	1	SHIELD BOX "B" (IN)	
38	1	SHIELD BOX "B" (OUT)	
37	1	SHIELD BOX "A" (OUT)	
36	1	SHIELD BOX "A" (IN)	
35	1	SHIELD BOX "A" (IN)	
34	1	SHIELD BOX "A" (OUT)	
33	1	BOX A (BOTT)	
32	1	BOX A (TOP)	
31	1	BOX A (BOTT)	
30	1	BOX A (TOP)	
29	1	BOX B (BOTT)	
28	1	BOX B (TOP)	
27	1	BOX B (BOTT)	
26	1	BOX B (TOP)	
25	1	BOX C (TOP)	
24	1	BOX C (BOTT)	
23	1	BOX C (BOTT)	
22	1	BOX C (TOP)	
21	1	FRAME III (BOTT)	
20	1	FRAME III (TOP)	
19	1	FRAME II (TOP)	
18	1	FRAME II (BOTT)	
17	1	FRAME I (BOTT)	
16	1	FRAME I (TOP)	
15	1	FRAME III (BOTT)	
14	1	FRAME III (TOP)	
13	1	FRAME II (BOTT)	
12	1	FRAME II (TOP)	
11	1	FRAME I (TOP)	
10	1	FRAME I (BOTT)	
9	1	BOX B FACE	
8	1	BOX B FACE	
7	1	BOX B FACE	
6	1	BOX C FACE	
5	1	BOX C FACE	
4	1	BOX C FACE	
3	1	BOX A FACE	
2	1	BOX A FACE	
1	1	BOX A FACE	THERMOCOUPLE

FIGURE 5 THERMOCOUPLE LOCATIONS

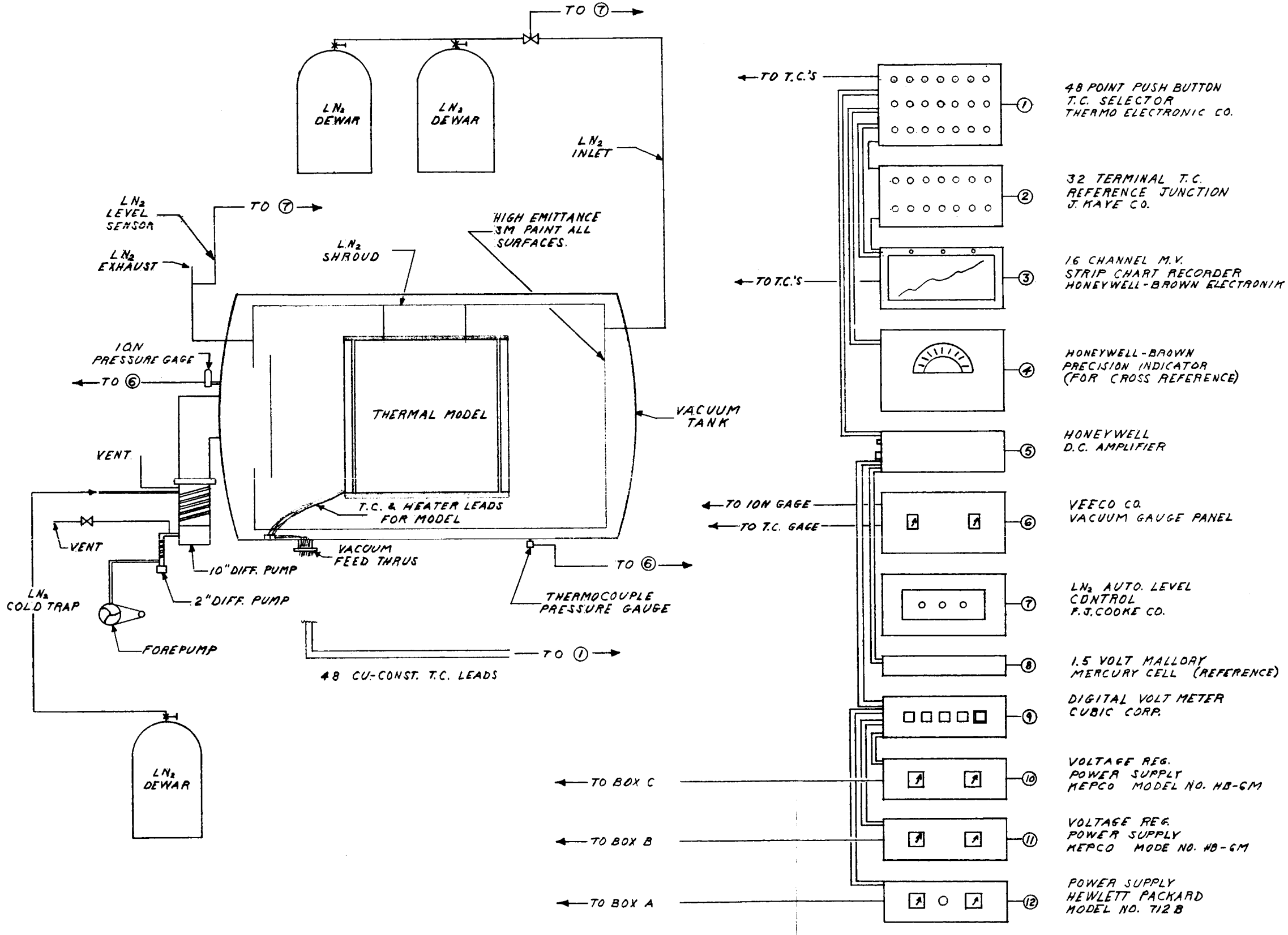

FIGURE 6 TEST CHAMBER AND INSTRUMENTATION

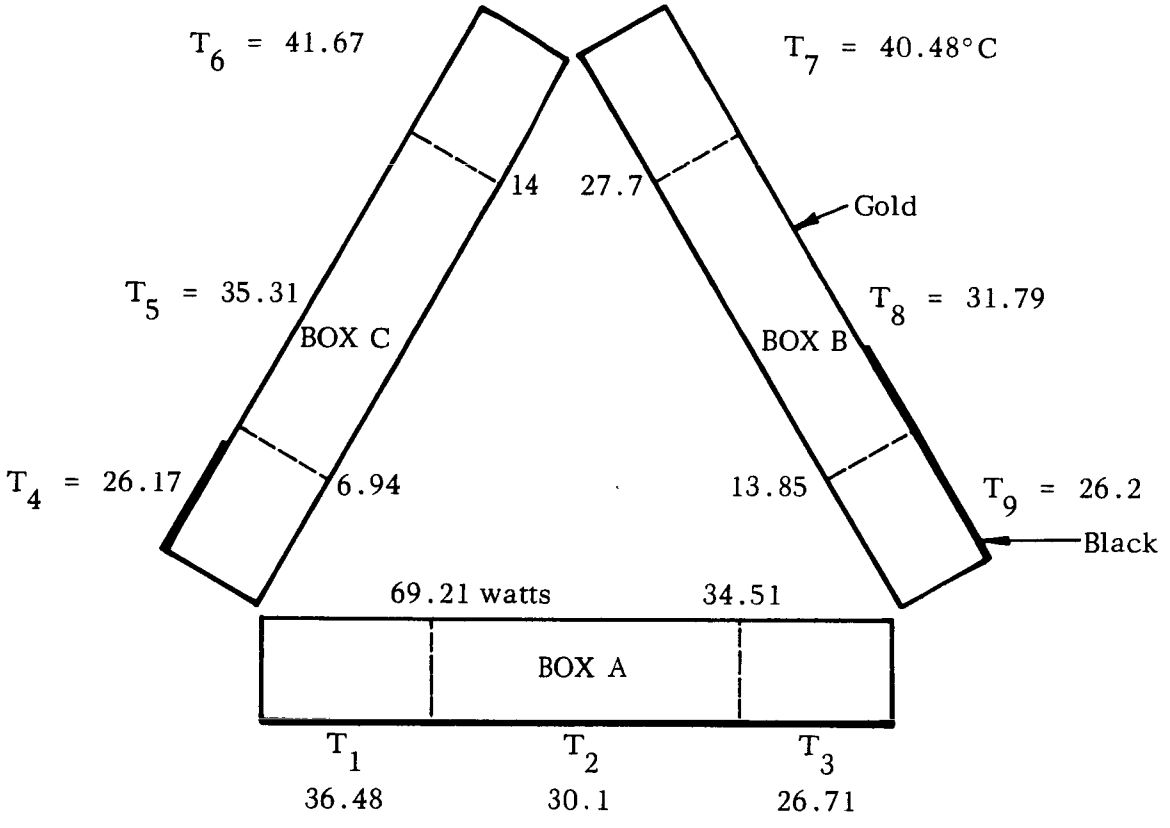

FIGURE 7 TYPICAL TEMPERATURE DISTRIBUTION: MODEL 1 - NORMAL POWER

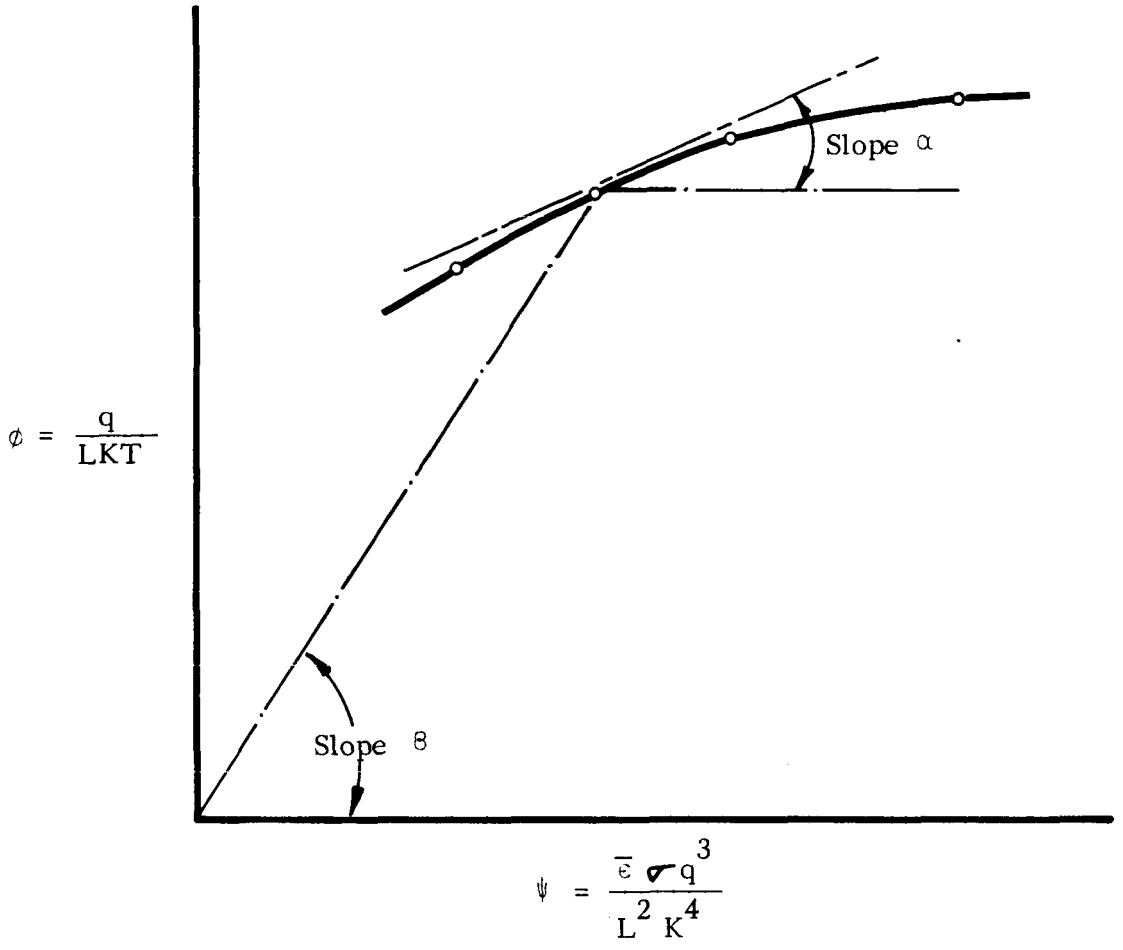

FIGURE 8 CORRELATION OF THERMAL MODEL TEMPERATURE DATA

APPENDIX I

CHEMICAL ANALYSIS OF MATERIALS

	C	Mn	P	S	Si	Cr	Ni	Cu	Mo
Armco Mag. Ingot Iron	.03	.02	.009	.016	-	-	-	-	-
HR E 4130 Steel	.32	.53	.010	.014	0.32	-	.06	1.01	.2
T304 HR Stainless	.05	1.0	.018	.020	.48	18.16	9.5	.12	.11

REFERENCES

1. Thermal Modeling of a Simulated JPL Spacecraft, Phase I Technical Report, Report to Jet Propulsion Laboratory by Arthur D. Little, Inc., Cambridge, Mass.

2. Powell, et al., Armco Iron as a Thermal Conductivity Standard, Progress in International Research on Thermodynamic Properties, ASME Publication, June 24, 1962.

3. Powers, et al., The Thermal Conductivity of Metals and Alloys at Low Temperatures, Ohio State University TR 264-6, April 25, 1951 (ATI-105923).